

Stochastic optimal control of open quantum systems

Aarón Villanueva* and Hilbert Kappen†

Radboud University, Heyendaalseweg 135, 6525 AJ Nijmegen, The Netherlands

January 16, 2025

Abstract

We consider the generic problem of state preparation for open quantum systems. As is well known, open quantum systems can be simulated by quantum trajectories described by a stochastic Schrödinger equation. In this context, the state preparation problem becomes a stochastic optimal control (SOC) problem. The SOC problem requires the solution of the Hamilton-Jacobi-Bellman equation, which is generally challenging to solve. A notable exception are the so-called path integral (PI) control problems for which one can estimate the optimal control solution by sampling. We derive a class of quantum state preparation problems that can be solved with PI control. We name the resulting algorithm Quantum Diffusion Control (QDC). By only requiring the propagation of state vectors ψ , QDC presents a quadratic advantage over density-centered approaches, such as PMP-based methods. Unlike most conventional quantum control algorithms, it does not require computing gradients of the cost function to determine the optimal control. Instead, it is computed by iterative importance sampling. The SOC setting allows in principle for a state feedback control solution, whereas Lindblad-based methods are restricted to open-loop control. We illustrate the effectiveness of our approach through some examples of open loop control for single- and multi-qubit systems.

1 Introduction

Effectively and efficiently controlling quantum systems to attain a desired behavior finds applications in quantum error correction [1], quantum simulation [2], quantum metrology [3], quantum sensing [4], state preparation [5], quantum state transfer [6] and quantum gate synthesis [7]. With recent increase in the experimental capabilities in measuring and manipulating quantum systems at the atomic, molecular and optical levels [8, 9, 10, 11, 12], developing efficient and scalable quantum control techniques has become an area of intense research [13, 14].

Control problems are generally classified into two categories: open-loop and closed-loop/feedback control. In feedback quantum optimal control (QOC), the controls depend on the system's state, requiring full or partial information about the state at each time. In contrast, open-loop QOC involves state-independent controls that are solely functions of time [15, 16]. Substantial study was dedicated to open-loop control for unitary dynamics. For such systems one formulates an open-loop QOC problem [17] which can be solved by using diverse methods, such as the paradigmatic gradient-based GRAPE algorithm [18] and its variants [19], search-based methods like CRAB [20], variational methods like Krotov optimization [21, 22, 23, 24] and techniques grounded in the Pontryagin Maximum Principle (PMP) [25]. These methods have been extensively applied to address a range of tasks [13, 14].

Control methods for open systems has been also a subject of intense study. For a review, consult [26]. Methods based on the Lindblad equation [27, 28, 29] can become computationally demanding for medium to large systems, as they require the evolution of density matrices, in contrast to wave functions in the unitary case. Moreover, these methods rely on local optimization as they are gradient-based. In some cases the gradients can be computed analytically or numerically [29]. But, in most cases, the gradients can only be computed approximately (such as in k -order Open GRAPE) and the gradient optimization can be difficult due to the temporal dependencies inherent in the control problem, an issue that occurs classically as well in dynamic programming [30]. Another limitation of these methods is that the optimal control is open-loop, not a feedback control, which can account for errors and

*aaronv@science.ru.nl

†b.kappen@science.ru.nl

stabilize the system. A feedback control is not possible in these frameworks due to the deterministic nature of the Lindblad equation, which treats the effects of noise on average.

In order to obtain a feedback control, the Lindblad equation needs to be replaced by a stochastic dynamics that explicitly models the effects of individual disturbances due to the environment and due to measurement. Such stochastic dynamics have been proposed under the name of *quantum trajectories* [31, 32, 33, 34] as stochastic generalizations of the Schrödinger equation. The Lindblad equation emerges then as the dynamics of the average $\langle \psi \psi^\dagger \rangle$ over quantum trajectories. Different ways of defining SSEs that lead to the same master equation constitute different *unravelings* of the master equation [35] and can take the form of a Markov jump process [31, 36, 37] or a diffusion process [38, 33, 39]. The mathematical framework was formulated by [40, 41, 42, 43]. Stochastic unravelings for non-Markovian scenarios can be traced back to Diosi [44] and Wiseman [45]. Quantum trajectories have been shown experimentally on different platforms, such as superconducting circuits [46, 47, 48, 49], optomechanical systems [50, 51] and hybrid quantum systems [52].

Control of open quantum systems using unravelings naturally results in a *stochastic optimal control problem* [53, 54, 42], where the optimal solution is a feedback control. See [55] for an introduction. The solution of the stochastic optimal control problem requires the solution of the Bellman equation or a stochastic version of PMP involving backward stochastic differential equations [56, 57], which in either case is very difficult in general. A notable exception are the linear quadratic Gaussian (LQG) problems, where the dynamics is linear in the state, the cost is quadratic in the control, and the noise is additive Gaussian. In general, the stochastic Schrödinger equation is not of the LQG form: it contains a bi-linear term $u\psi$, with u the control and ψ the quantum state, and it may contain more non-linearities due to a state normalization constraint. However, the bi-linearity does not necessarily preclude the formulation of an LQG control problem in the Heisenberg picture [55], and this has been used to control quantum systems. It was demonstrated for cooling and position localization of a quantum particle [58, 59], the cooling of the vibrations of a mechanical resonator [9] and the position of an optically trapped nano particle at room temperature [12].

The feedback control requires information about the quantum state through *measurement*. Since the quantum state is only partially observable through measurement, the control problem becomes what is known as a *partial observable control problem* [60]. A unique quantum feature, not present in classical systems, is that measurement will disrupt the quantum state by projecting the state onto one of the measurement eigenstates (quantum back-action). A compromise between information gain and minimal disruption of the quantum state is given by the so-called *weak or continuous measurement* [61, 62, 63]. The issue of partial observability and measurement is not so important for LQG control problems, because of a property called certainty equivalence, which essentially states that the optimal control depends on the expected latent state only. However, partial observability and the correct treatment of measurement becomes important for stochastic optimal control problems beyond the LQG regime.

Measurement can be elegantly formalized by the so-called hybrid dynamics, which describes the simultaneous time evolution of the quantum state and the classical observation(s) [64]. The theory of unravelings of the hybrid dynamics in terms of discrete time quantum jumps was first developed by [65]. Its generalization to continuous time measurements was recently proposed as a theoretical framework to unify quantum physics with gravity [66, 67] and generalizes earlier work on continuous measurement by [68, 69].

Although the theory of stochastic optimal control of quantum systems is well developed, its application has so far been mostly restricted to the LQG case. There exists another class of control algorithms that can solve a large class of non-linear stochastic optimal control problems, known as the path integral (PI) control method [70, 71, 72]. This presents a quite large class of stochastic optimal control problems with non-linear dynamics, non-Gaussian noise and non-linear control cost. A strong requirement for the control problem to be of the PI form is that the noise dW and the control $u dt$ should appear in the dynamics as their sum $u dt + dW$. The advantage of the PI control problem is that the optimal control solution can be expressed in closed form as a path integral, without needing to solve the Bellman or PMP equations. The path integral can be estimated relatively efficiently through sampling. The sampling is optimized using a procedure called adaptive importance sampling which estimates gradients based on self-generated quantum trajectories [71] and is well suited for parallel computing with virtually no overhead. PI control has been very successfully applied to many high dimensional non-linear stochastic optimal control problem with real-time requirements that occur in robotics where all other methods fail [73]. See [74] for a recent review of the PI method and related work.

In this paper we propose to apply the PI control method to control an open quantum system whose dynamics can be written in Lindblad form. To simulate the Lindblad equation, we use continuous unravelings that yield a quantum diffusion process and that is formulated as stochastic differential equations (SDE) with Brownian noise.

These unravelings are not unique and in general not of the PI control form. For certain combinations of control Hamiltonian and Lindblad operators we can use this freedom to define a PI control problem. We consider the problem of quantum state preparation. This problem can be formalized as a finite-horizon stochastic optimal control problem that can be efficiently solved using the PI control method. In this paper, we will focus on open loop control because closed-loop control requires the inclusion of quantum measurement in the unravelings, which is a topic that we will consider in the future. To our knowledge, this is the first attempt in combining state-centered quantum trajectories techniques with path integral control theory.

This paper is organized as follows. In Section 2, we provide the necessary background knowledge of continuous-time unravelings of the Lindblad equation. In Section 2.1, we define a class of transformations on the Lindblad operators and the noise matrix that leaves the Lindblad equation invariant while changing the unraveling. This transformation proves instrumental for mapping many interesting control problems originally formulated in Lindblad form onto stochastic optimal control problems of the PI form. In Section 3, we review the main results from path integral control theory. The optimal control that results from solving the path integral equations is a feedback control, i.e. it depends on the system state. In practice, computing the optimal control exactly can be challenging if not unfeasible due to the infinite dimensionality of the control. In Section 3.1, we use an importance sampling scheme to approximate the optimal control by a surrogate model based on linear combinations of arbitrary basis functions. In Section 4, we present our quantum control algorithm by combining quantum unravelings with path integral control. In Section 5, we show some proof-of-principle numerical examples of state preparation. In Sections 6 and 7, we close with discussions about the challenges and prospects of future work.

2 Unravelings of the Lindblad equation

Here we study systems whose dynamics can be described by the Lindblad equation [75]¹

$$\dot{\rho} = -i[H, \rho] + \mathcal{D}[D, C]\rho \quad \mathcal{D}[D, C]\rho := D_{ab} \left(C_a \rho C_b^\dagger - \frac{1}{2} \{C_b^\dagger C_a, \rho\} \right) \quad (1)$$

where \mathcal{D} denotes the dissipation superoperator, H is the system's Hamiltonian and $C_a, a = 1, \dots, n_c$ are the Lindblad operators. The noise matrix D is assumed to be positive semidefinite. This is a sufficient condition, although not necessary [76], for ensuring positive evolution maps. Here we restrict D to be real symmetric.

The Lindblad equation can be interpreted as an average dynamics obtained from considering all particular time realizations of the quantum state ψ . This leads to the theory of stochastic unravelings. Stochastic quantum unravelings are usually encoded as a stochastic differential equation (SDE) of the state ψ . The SDE is designed in such a way that the density operator $P = \psi\psi^\dagger$, a stochastic variable, follows in average a Lindblad evolution, i.e. $\rho = \langle \psi\psi^\dagger \rangle$, with ρ satisfying (1). One can define unravelings in many ways, for instance using stochastic jumps at discrete times or using continuous Wiener noise. In this work we use the latter. Assume the following SSE

$$d\psi = -iH\psi dt - \frac{1}{2}D_{ab} \left(C_b^\dagger C_a - 2c_a C_b + c_a c_b \right) \psi dt + (C_a - c_a)\psi dW_a \quad (2)$$

with dW_a a real-valued Wiener process with $\langle dW_a \rangle = 0$ and $\langle dW_a dW_b \rangle = D_{ab} dt$, with D a symmetric matrix. The C_a are the Lindblad operators appearing in (1) and $c_a := \psi^\dagger C_a^{(h)} \psi$ with $C_a^{(h)} := \frac{1}{2} (C_a + C_a^\dagger)$, the Hermitian part of C_a . Given these definitions, one can state the following result.

Proposition 1. *Eq. (2) is an unraveling of the Lindblad equation (1).*

For the proof we remit the reader to Appendix A. See also [33, 77, 55, 78] for previous derivations of this result. The specific form of (2) is not arbitrary and its derivation satisfies very general physical constraints. If one considers that the term $C_a \psi dW_a$ in (2) implements the basic stochastic action from the environment onto the quantum state, then the remaining terms are needed to ensure that ψ remains normalized under the dynamics ($d\|\psi\|^2 = 0$). The c_a terms introduce non-linearities in the dynamics. This is a natural consequence of the stochastic non-Hermitian interaction of the system with the environment, which makes the evolution non-unitary and, therefore, violates norm preservation. A non-unitary norm preserving dynamics is necessarily non-linear.

¹Along the text, repeated indices denote summation convention unless we explicitly state the contrary.

2.1 Invariance of the Lindblad equation

Consider the Lindblad equation (1) with m Lindblad operators C_a , $a = 1, \dots, m$. We assume that the C_a are linearly independent. They therefore span a m -dimensional space of operators \mathcal{S} and the C_a form a (generally non-orthogonal) basis for \mathcal{S} . Given an $m \times m$ invertible complex-valued matrix A , define the following linear transformation on the Lindblad operators C_a and the noise matrix D ,

$$\tilde{C}_b = C_a A_{ab} \quad D = A \tilde{D} A^\dagger \quad (3)$$

This linear transformation leaves the dissipation operator (and, therefore, the Lindblad equation (1)) $\mathcal{D}[D, C]$ invariant

$$\mathcal{D}[D, C] = \mathcal{D}[\tilde{D}, \tilde{C}]. \quad (4)$$

On the other hand, transformation (3) changes the form of the SSE (2). Thus, the gauge freedom induced by transformation (3) gives rise to an infinite class of different but equivalent quantum unravelings simulating the same Lindblad equation. Obviously, this freedom allows for the design of different unravelings that can be more or less convenient depending on the problem we want to solve. In particular, if we can find a transformation A that leaves \tilde{C}_a ($a = 1, \dots, m$) anti-Hermitian and \tilde{D} real symmetric, then the non-linear terms $\tilde{c}_a = \psi^\dagger \tilde{C}_a^{(h)} \psi = 0$, and the unraveling of the Lindblad equation in terms of the \tilde{C}_a and \tilde{D} is both linear and norm-preserving.

$$d\psi = -iH\psi dt - \frac{1}{2}\tilde{D}_{ab}\tilde{C}_b^\dagger\tilde{C}_a\psi dt + \tilde{C}_a\psi d\tilde{W}_a \quad \langle d\tilde{W}_a d\tilde{W}_b \rangle = \tilde{D}_{ab}dt \quad (5)$$

For instance, when all C_a are Hermitian, the unraveling (2) is non-linear with $c_a = \psi^\dagger C_a \psi$. Using (3) with $A_{ab} = i\delta_{ab}$ gives $\tilde{C}_a = iC_a$ anti-Hermitian and $\tilde{D} = D$, and the unraveling is linear.

The transformation to a basis of anti-Hermitian operators is clearly not always possible. A necessary condition is that the space \mathcal{S} must contain anti-Hermitian operators. Take the case $m = 1$, where C_1 is neither Hermitian nor anti-Hermitian. The operator \tilde{C}_1 cannot be made anti-Hermitian for any A . For a non-trivial example, see Section 5.1.

As we will see in the following, the transformation to anti-Hermitian operators turns out to be essential to cast the control of the unravelings as a path integral control problem. The fact that the unravelings also become linear in this case is a complimentary bonus.

3 The path integral control method

We briefly review the path integral control theory [70] in its most general form. See [72] for details. Consider a dynamical system of the form

$$dX_t^u = f(t, X_t^u)dt + g(t, X_t^u)(u(t, X_t^u)dt + dW_t) \quad (6)$$

for $t_0 \leq t \leq T$ with $X_{t_0}^u = x_0$. Here W_t is a m -dimensional real Brownian motion with $\langle dW_t^a \rangle = 0$ and $\langle dW_t^a dW_t^b \rangle = \nu^{ab}dt$ with ν a $m \times m$ positive symmetric matrix. We take $f : [t_0, T] \times \mathbb{R}^n \rightarrow \mathbb{R}^n$, $g : [t_0, T] \times \mathbb{R}^n \rightarrow \mathbb{R}^{n \times m}$ and $u : [t_0, T] \times \mathbb{R}^n \rightarrow \mathbb{R}^m$. Given the function $u(t, x)$ that defines the control for each state x and each time t , we define the cost²

$$S^u(t) = \Phi(X_T^u) + \int_t^T \left[V(s, X_s^u)ds + \frac{1}{2}u(s, X_s^u)^T R u(s, X_s^u)ds + u(s, X_s^u)^T R dW_s \right] \quad (7)$$

with X_t^u the stochastic solution of (20) at time t . The matrix R is positive $m \times m$ symmetric such that $R = \lambda \nu^{-1}$ with $\lambda > 0$ a constant. The function V is the state-dependent path cost and Φ the end cost. The control problem is to find the function u that minimizes

$$J(t_0, x_0) = \min_u \langle S^u(t_0) \rangle \quad (8)$$

²Note, that the expectation of the last term in (7) vanishes, but this term is needed later when deriving the optimal solution of the path integral theory.

where $\langle \cdot \rangle$ denotes the average over all possible realizations $X_{t_0:T}^u$ conditioned on $X_{t_0}^u = x_0$. The function $u^* : [t_0, T] \times \mathbb{R}^n \rightarrow \mathbb{R}^m$ that minimizes (8) is called the optimal control.

The generic approach to solve a stochastic optimal control problem is to derive a partial differential equation for $J(t, x)$, known as the Bellman equation, from which one computes the optimal control (see proof of Lemma 1 in Appendix B). For the class of control problems defined above, one can establish the following result.

Theorem 1. *The optimal cost-to-go and optimal control of the control problem with dynamics (6) and cost (7) and (8) is given by*

$$J(t_0, x_0) = -\lambda \log \left\langle e^{-S^u(t_0)/\lambda} \right\rangle \quad (9)$$

$$\hat{u}(t_0, x_0) = u(t_0, x_0) + \lim_{dt \rightarrow 0} \frac{1}{dt} \frac{\langle e^{-S^u(t_0)/\lambda} W_{t_0+dt} \rangle}{\langle e^{-S^u(t_0)/\lambda} \rangle} \quad (10)$$

Proof. The proof is given in [72] and reproduced in Appendix B, where (9) follows directly from Corollary 2 by taking $t = t_0$, and the proof of (10) is established in Corollary 4. \square

Theorem 1 gives an explicit solution of the optimal cost-to-go and optimal control at t_0, x_0 in terms of path integrals. Therefore the optimal control solution can be obtained by sampling. The control function u is referred to as the sampling control. Note that the l.h.s. of Eqs. (9) and (10) are independent of u : The result holds for any sampling control u , for instance the naive sampling control $u(x, t) = 0$. However, naive sampling strategies yield estimates with large statistical variance.

In Eqs. (9) and (10), the cost of the i -th sample trajectory is given by $S_i^u(t_0)$. Each trajectory is weighted by $w_i = \frac{e^{-S_i^u(t_0)/\lambda}}{\sum_{i=1}^{N_{traj}} e^{-S_i^u(t_0)/\lambda}}$, with N_{traj} the total number of trajectories. When $S_i^u(t_0)$ has large variance, the batch of samples is dominated by one sample: the sample with lowest $S_i^u(t_0)$, in particular for low λ (i.e. low noise). The quality of the sampling can be quantified by the effective sample size [72]

$$ESS := N_{\text{eff}}/N_{traj}, \quad N_{\text{eff}} := \left(\sum_{i=1}^{N_{traj}} w_i^2 \right)^{-1} \quad (11)$$

where $1/N_{traj} \leq ESS \leq 1$ and reaches its maximal value $ESS = 1$ when $N_{\text{eff}} = N_{traj}$ with all samples having equal weight $w_i = 1/N_{traj}$. In [72], it was shown that sampling controls with lower control cost (8) are better samplers in the sense of smaller statistical variance and larger ESS . The optimal sampling control is given by the optimal control solution with minimal cost of J in (8): When u is the optimal control solution, the variance of $S^u(t_0)$ is zero, $w_i = 1/N_{traj}$ and $ESS = 1$. Thus any u implements an importance sampler, that is, an unbiased estimator of J and \hat{u} , but with different quality in terms of statistical variance. This is the basic idea of iterative importance sampling, discussed in Section 3.1.

The quality of the control solution is in principle given by the value of the control cost J in (8). Because of the monotonic relation between control cost and effective sample size, one can also measure the quality of the control solution in terms of ESS instead of J , which turns out to be a more sensitive measure of optimality.

3.1 Iterative importance sampling

In practice, we need to estimate the optimal control at all spacetime points (t, x) , not just at the initial conditions (t_0, x_0) . For this, it is useful to parametrize the control functions \hat{u} and u . Here, we consider linear parametrizations

$$\hat{u}_a(t, x) = \sum_{k \in I} \hat{A}_{ak} h_k(t, x), \quad u_a(t, x) = \sum_{k \in I} A_{ak} h_k(t, x) \quad a = 1, \dots, n_c \quad (12)$$

where \hat{A}_{ak}, A_{ak} are constants and $h_k : [t_0, T] \times \mathbb{R}^m \rightarrow \mathbb{R}$ are fixed basis functions. The symbol I denotes the index set labeling the basis functions.

Using Theorem 3 (App. B) with $f(t, x) = h_{k'}(t, x)$ we obtain the matrix equation

$$\sum_k (\hat{A}_{ak} - A_{ak}) B_{kk'} = C_{ak'} \quad (13)$$

with

$$B_{kk'} = \left\langle e^{-S^u(t_0)/\lambda} \int_{t_0}^T h_k(t, X_t^u) h_{k'}(t, X_t^u) dt \right\rangle \quad C_{ak} = \left\langle e^{-S^u(t_0)/\lambda} \int_{t_0}^T h_k(t, X_t^u) dW_t^a \right\rangle \quad (14)$$

The statistics $B_{k_1 k_2}$ and C_{ak} can be estimated simultaneously using one batch of sample trajectories. Eq. (13) can be solved for the matrix \hat{A} in terms of the matrices A, B and C by matrix inversion:

$$\hat{A} = A + CB^{-1} \quad (15)$$

Eq. (15) gives an approximation to the optimal control solution in terms of the sampling control A and the expectations B, C , which are estimated by sampling with sampling control u .

One can iteratively apply (15) using the \hat{A} that is computed at iteration p as the sampler for iteration $p + 1$. This is called adaptive importance sampling (IS) and (15) takes the form

$$A^{p+1} = A^p + C^p (B^p)^{-1} \quad (16)$$

The procedure can be initialized for instance with $A_0 = 0$ or any other value³.

A piece-wise constant open-loop control ($u_a(t, x) = u_a(t)$) is obtained as follows. Consider the K intervals $I_k = [\tau_{k-1}, \tau_k]$ with time points $t_0 = \tau_0, \tau_1, \dots, \tau_K = T$. Define h_k in (12) as the indicator functions $h_k(t) = \delta_{t \in I_k}$. The adaptive importance sampling equation becomes

$$A_{ak}^{p+1} = A_{ak}^p + \frac{\left\langle e^{-S^u(t_0)/\lambda} \int_{I_k} dW_t^a \right\rangle_p}{\Delta\tau_k \left\langle e^{-S^u(t_0)/\lambda} \right\rangle_p} \quad k = 1, \dots, K \quad (17)$$

with $\Delta\tau_k = \tau_k - \tau_{k-1}$ and $\langle \cdot \rangle_p$ the statistics computed with control A^p . These expectations are estimated from N_{traj} stochastic trajectories.

From our numerical experiments we find that the adaptive importance sampling finds better solutions when a form of smoothing is introduced: we replace A_{ak}^p on the right hand side of (17) (in both terms) by a its recent average over a window of past IS steps: $\frac{1}{w} \sum_{p'=p-w+1}^p A_{ak}^{p'}$ with w the window size. However, smoothing results in a slower convergence of the algorithm.

4 Path integral control of open quantum systems

We now consider the state preparation problem. We want to prepare a quantum state from a given initial state in total time T , but want to do so by including the effects of the interaction of the system with its environment. For this, we assume the system dynamics follows the Lindblad equation (1). One can formulate this as a finite horizon control problem where the Hamiltonian in (1) takes the form $H = H_0 + u_a H_a$ with $H_a (a = 1, \dots, n_c)$ a set of Hermitian operators and $u_a (a = 1, \dots, n_c)$ real-valued control fields. Given the time interval $[0, T]$, we define the control objective as

$$C[u] = -\frac{Q}{2} \mathcal{F}(\rho_T) + \frac{1}{2} \int_0^T u_t^T R u_t dt \quad (18)$$

where ρ_T represents the quantum state at the final time T , Q is a positive constant and R is a real symmetric positive $n_c \times n_c$ matrix. The objective is composed of two parts. The first term is the fidelity $\mathcal{F}(\rho_T) = \text{Tr}(\rho_T \phi \phi^\dagger)$ of the final state ρ_T with respect to a target (pure) state ϕ . The second term is an energy constraint and it penalizes the accumulated magnitude of the different controls. We want to find the optimal control u^* that minimizes the objective function (18):

$$u^* = \underset{u}{\text{argmin}} C[u]$$

Eqs. (1) and (18) define a deterministic control problem and the optimal control solutions u_a are state-independent functions. As we mentioned earlier, this is referred to as open-loop control and it can be approached by using for example the PMP method [25].

³For instance, with the solution of the corresponding deterministic control solution ($D = 0$) that can be efficiently obtained using PMP or GRAPE.

Here instead, we propose to consider the stochastic optimal control problem based on the unravelings of the Lindblad equation. For this, consider the following cost functional

$$C = \left\langle -\frac{Q}{2}\mathcal{F}(\psi_T) + \frac{1}{2}\int_0^T u_t^T R u_t dt \right\rangle \quad (19)$$

where ψ_t is the quantum state satisfying the SSE (2) and $\mathcal{F}(\psi) = \text{Tr}(\psi\psi^\dagger\phi\phi^\dagger)$. When the controls depend on the state, the problem is referred to as closed-loop/feedback control. These control problems can be solved using the PI control formalism when the Lindblad operators C_a can be transformed into anti-Hermitian operators $-iH_a$ using the transformation (3), while maintaining a real symmetric covariance matrix, as discussed in Sec. 2.1. When the transformation is possible, the unraveling is linear and norm-preserving and the SSE takes the form

$$d\psi = -iH_0\psi dt - \frac{1}{2}\tilde{D}_{ab}H_aH_b\psi dt - iH_a\psi(u_a dt + d\tilde{W}_a) \quad \langle d\tilde{W}_a d\tilde{W}_b \rangle = \tilde{D}_{ab}dt \quad (20)$$

In addition, the transformation should leave the cost (19) invariant. The first term is invariant because $\langle \text{Tr}(\psi_T\psi_T^\dagger Q) \rangle = \text{Tr}(\rho_T Q)$ and ρ_T is invariant. The second term is generally not invariant, except when u is open loop, as there is no state dependence in that case. For feedback control, the stochastic optimal control formulation depends on the specific unraveling employed.

The control problem defined by Eqs. (20) and (19) is in path integral form ⁴ as discussed in Section 3 provided that $R\tilde{D} = \lambda I$ with I the identity matrix and $\lambda > 0$. The open loop control solution can therefore be estimated using the adaptive importance sampling algorithm given by (17). We refer to this algorithm as Quantum Diffusion Control (QDC).

5 Numerical experiments

In this section we demonstrate through several examples the practicality and flexibility of our algorithm in solving different quantum control problems of interest. For all the experiments we use piece-wise constant (PWC) open loop controls over K time intervals. We parametrize the controls according to (12) and write

$$u_a(t) = \sum_{k=1}^K u_{ak}\delta_{t \in I_k} \quad a = 1, \dots, n_c \quad (21)$$

where $I_k = [\tau_{k-1}, \tau_k]$, u_{ak} is the k -th pulse corresponding to control u_a , and n_c is the number of controls. We use the Euler-Maruyama integration scheme for simulating the stochastic dynamics (20).

5.1 Control of a noisy qubit

Consider a single-qubit system evolving according to the Lindblad equation (1) with $H = u_x H_x + u_y H_y$, where $H_x = \sigma_x$ and $H_y = \sigma_y$. The dissipation part is given by the two non-Hermitian operators $C_1 = \sigma^+$ and $C_2 = \sigma^-$, where $\sigma^\pm = \frac{1}{2}(\sigma_x \pm i\sigma_y)$. This system is commonly used for modeling the emission and absorption of light quanta in a two-level system coupled to an electromagnetic field, e.g. a cavity resonator [34]. Assume a diagonal noise matrix $D_{ab} = D\delta_{ab}$. The Lindblad equation is

$$\dot{\rho} = -i[H, \rho] + D(\sigma^+\rho\sigma^- + \sigma^-\rho\sigma^+ - \rho) \quad (22)$$

⁴This can be easily seen. The dynamics in (20) is of the form

$$d\psi = f dt + g_a(u_a dt + dW_a)$$

with complex valued vector functions f and g_a . We write $d\psi, f, g_a$ in terms of their real and imaginary components $j = r, i$:

$$d\psi^j = f^j dt + g_a^j(u_a dt + dW_a)$$

which is already in path integral form.

To propose an unraveling suitable for PI formulation, we transform the dissipators to a pair of anti-Hermitian operators using (3) with $\tilde{C}_1 = -iH_1, \tilde{C}_2 = -iH_2$ and

$$A = \begin{pmatrix} -i & -1 \\ -i & 1 \end{pmatrix} \quad (23)$$

and $\tilde{D}_{ab} = \frac{1}{2}D\delta_{ab}$. The unraveling (20) becomes:

$$d\psi = -\tilde{D}\psi dt - i\sigma_a\psi(u_a dt + dW_a) \quad (24)$$

where $a = x, y$. As stated in Sec. 2, this unraveling preserves the norm of ψ . This implies that the stochastic trajectories generated by (24) lie on the Bloch sphere.

We use as cost Eq. (19), subject to $R\tilde{D} = \lambda$. We consider the state preparation problem from an initial state $\psi_0 = |X\rangle := \frac{1}{\sqrt{2}}(|0\rangle + |1\rangle)$ to a target state $\phi = |Y\rangle := \frac{1}{\sqrt{2}}(|0\rangle + i|1\rangle)$. Although the transformation $X \rightarrow Y$ can be realized by a simple σ_z rotation, this task is challenging, since σ_z is not one of the control primitives in H . Instead, σ_x, σ_y must coordinate so as to realize the desired rotation. As a result, the optimal trajectories do not lie on the equator.

In Fig. 1 (A) we show the adaptive importance sampling. We plot the average fidelity over trajectories F_{avg} , the worse case fidelity over trajectories F_{min} and the average control cost C in (19) versus IS steps. In addition, we plot the effective sample size ESS in (11), which is a sensitive measure of the quality of the optimal control solution. The ESS indicates how close the control solution is to the optimal (feedback) control, for which $ESS = 1$. We observe that while the fidelity and control cost converge fast to constant values, the ESS still increases indicating that the quality of the control solution is still improving (shaded region). We observe that the control solution becomes smoother in these later IS iterations. The asymptotic average fidelity for $K = 128$ is $F^* = 0.9759 \pm 0.0006$. Since the optimal control solution is a compromise between the final fidelity and the fluence $U := \int_0^T u^T(t)u(t)$, higher fidelity solutions can be obtained by lowering R in Eq. (19). Indeed, by reducing $R = 1$ to $R = 0.1$ the average asymptotic fidelity increases to $F^* = 0.9963 \pm 0.0002$. Fig. 1 (B) shows one of the two optimal control solutions $u_{x,y}(t)$ after convergence of the IS training. The other solution is obtained by taking $u_{x,y}(t) \rightarrow -u_{x,y}(t)$. In Fig. 1 (C) we show how the quality of the optimal control solution in terms of asymptotic ESS depends on the number of pulses K . The ESS increases monotonically until reaching an asymptote at around $ESS \sim 0.21$, showing the sub-optimality of the open-loop control compared to the optimal feedback solution (for which $ESS = 1$). Fig. 1 (D) shows quantum trajectories on the Bloch sphere under optimal control.

Benchmark with Open GRAPE.— As benchmark, we compare the performances of QDC and (first order) Open GRAPE algorithm [27], which computes coherent controls for the Lindblad equation. See Appendix C for details on the algorithm and implementation. We solve the state preparation problem $X \rightarrow Y$ for the single qubit using $K = 128$ pulses. The control problem is defined by the Lindblad equation (22) and the cost function (18).

We run QDC and Open GRAPE algorithms 505 times using random control initializations drawn from both normal and uniform distributions. Regarding the stopping condition for Open GRAPE, the optimization stops when the cost cannot be further optimized by decreasing the learning rate; see App. C for details. In the case of QDC algorithm, the optimization runs for a maximum of 800 IS steps, ensuring that the algorithm reaches convergence in every run.

In Fig. 2 we show the distribution of control costs (along the fidelities and fluences) for Open GRAPE (main panels) and QDC (insets). We mark the average cost, fidelity and fluence of QDC solutions by a yellow dot in each graph. The QDC solutions have lower cost than the Open GRAPE solutions. The width of the dashed vertical lines locating each mean is much larger than the standard deviation of each QDC distribution, showing that the variance of QDC solutions is very narrow compared to that of Open GRAPE ones. Open GRAPE converges to many different solutions with different costs depending on the initial condition. Instead, QDC converges consistently to one of two solutions with same cost, fidelity, fluence and effective sample size, which are related by a global sign (Fig. 1 (B)). The difference between individual solutions has RMS error less than $\mathcal{O}(10^{-4})$. By direct inspection we can also verify that these profiles correspond to two different underlying smooth solutions. We conclude that the different QDC solutions, rather than representing local minima, correspond to the same underlying solution up to small statistical fluctuations due to the stochastic nature of the algorithm. We further compare these two algorithms' solutions by performing a t-SNE embedding [79] over Open GRAPE solutions together with QDC solutions. In Fig. 3 (A) we plot some of the most regular Open GRAPE control solutions. In Fig. 3 (B) we show the t-SNE

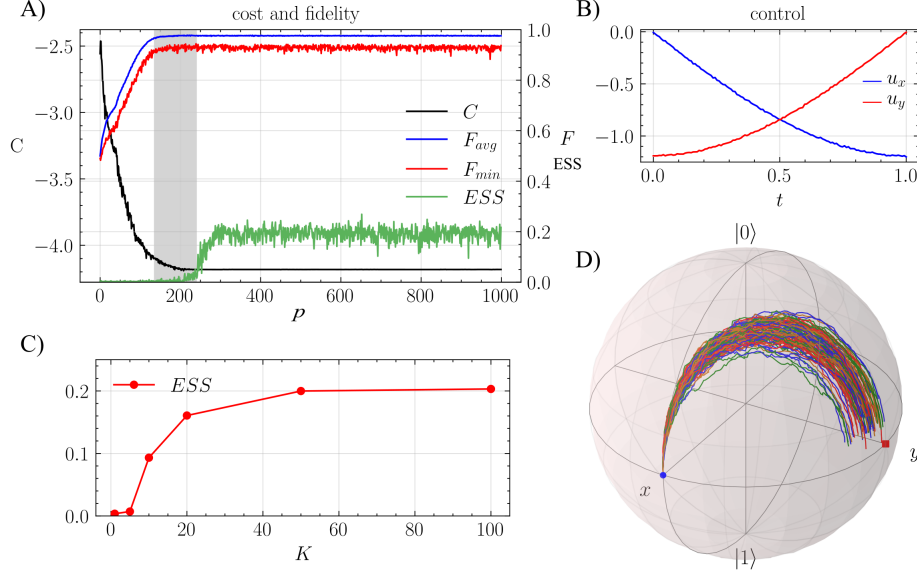


Figure 1: Control of a noise qubit from $X \rightarrow Y$. (A) Average fidelity F_{avg} , minimal fidelity F_{min} , effective sample size ESS and cost C in 19 versus importance sampling iterations p . The converged average fidelity is $F^* = 0.9759 \pm 0.0006$. (B) Optimal control solution $u_{x,y}(t)$ after convergence of the algorithm. The optimal solution is two-fold degenerate. The two solutions are related by a global sign $u_{x,y} \rightarrow -u_{x,y}$. (C). Dependence of the quality of the optimal control, measured by the ESS , on the number of pulses K . (D). Optimally controlled trajectories on the Bloch sphere. Parameters: final time $T = 1$, noise coupling $D = 0.005$, control weight $R = 1$, fidelity weight $Q = 10$, number of pulses $K = 128$, number of trajectories $N_{traj} = 400$ per IS step, maximum number of importance sampling (IS) steps $n_{IS} = 1000$ and time discretization $dt = T/N_T$ with $N_T = 128$. IS smoothing window $w = 40$ (see Section 3.1).

embeddings for $[u_x, u_y]$, considered as a vector of length $2K$. Each dot represent a different Open GRAPE solution and we represent the (average) QDC solutions with yellow dots. We further perform a K-means decomposition to cluster the different solutions into 3 clusters (colored with red, blue and black). The different Open GRAPE solutions tend to cluster around each ground truth QDC solution. In Fig. 3 (C) we plot the average profiles of the Open GRAPE solutions of cluster 1 (red) and cluster 2 (blue) together with the average QDC profiles. The qualitative resemblance between the averages and the QDC solution indicates that the Open GRAPE local minima tend to cluster around the ground truth solutions represented by QDC solutions. The cluster colored with black consists of local minima control solution of Open GRAPE with high control cost C .

During the IS iterations of the QDC algorithm, the optimization keeps improving in terms of ESS , even when maximum fidelities are reached; see shaded area in Fig. 1. Instead, Open GRAPE solutions, while having similar fidelities as the QDC solution, have low $ESS = \mathcal{O}(10^{-3})$. We expect that the high fidelity, high- ESS QDC solutions are more robust to random perturbations than the high fidelity, low- ESS Open GRAPE solutions. We test this by perturbing the optimal control solution $u(t) \rightarrow u(t) + \xi(t)$ with $\xi(t)$ with Gaussian perturbations with mean zero and standard deviation σ and compute the maximal cost difference $\Delta C = C(u + \xi) - C(u)$ for 20 different noise realizations. We compare high-fidelity low- ESS Open GRAPE solutions, defined by having a cost $C < -3.8$ with the high fidelity high ESS QDC solution in Fig. 3 (D) for different σ . For completeness, we also include in the experiment the high-fidelity low- ESS QDC solutions corresponding to the shaded area of Fig. 1 (A). It can be observed that the QDC solution (in red) is more robust to random perturbations than low- ESS Open GRAPE solutions (in black). Therefore, we conclude that the ESS is a useful additional criterion to assess the quality in terms of the robustness of the (open loop) control solution.

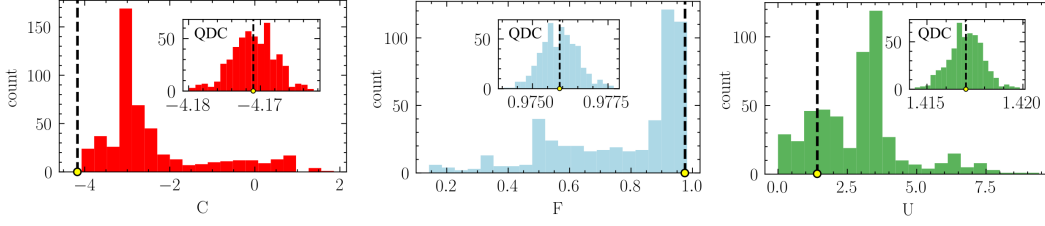


Figure 2: Histograms of optimal control costs obtained with Open GRAPE (main panel) and QDC (inset) on 505 runs. For Open GRAPE, the average cost, fidelity and fluence (and standard deviations) are $\langle C \rangle = -4 \pm 1$, $\langle F \rangle = 0.8 \pm 0.2$ and $\langle U \rangle = 3 \pm 2$, respectively. The minimum cost achieved is $C_{min} = -4.07$. For QDC, the corresponding average values (yellow dot) are $\langle C \rangle = -4.171 \pm 0.003$, $\langle F \rangle = 0.9759 \pm 0.0006$ and $\langle U \rangle = 1.4170 \pm 0.0009$. In the main panels, the dashed vertical lines at the QDC average are wider than the actual standard deviations of the QDC distributions. This illustrates the large difference in variance between the two methods. All QDC runs converge to solutions with the same cost, fidelity, fluence and effective sample size up to small statistical fluctuations due to the stochastic nature of QDC algorithm. Parameter setting: $D = 0.005$, $T = 1$, $R = 1$, $Q = 10$, $K = 128$, $w = 20$.

5.2 Leveraging open-system solutions for unitary dynamics

The dynamics of the average state $\langle \psi \rangle$ follows the equation

$$d \langle \psi \rangle = -i(H_e + H_u) \langle \psi \rangle dt \quad (25)$$

where $H_e = H_0 - \frac{i}{2} D_{ab} H_a H_b$ and $H_u = u_a H_a$. Provided that the norm of the correction term $D_{ab} H_a H_b$ is sufficiently small, we expect the solution of the open control problem to work well for the unitary case $D = 0$. Conversely, we expect this correspondence to degrade as D increases. The question is then to which extent we can leverage the solution of the open control problem to achieve high fidelities in the unitary case.

We explore this question for the noisy qubit. We compare the fidelity scores for the open and closed system for different noise values D . We consider the $X \rightarrow Y$ state preparation problem. For each D , we compute a control u that achieves maximal average fidelity F_{open} for the open case, and use it to steer the unitary dynamics in the time interval $[0, T]$. Then, we compare F_{open} with the fidelity achieved at time T in the unitary case, which we denote F_{closed} . See Fig. 4 (A).

Surprisingly, the unitary dynamics reaches high fidelities for a wide range of noise values, even when F_{open} deteriorates fast as D increases. Moreover, both, the open and the unitary dynamics, show a sharp transition in the fidelity at a certain noise value D_c . This point also corresponds with a fast decrease in the fluence. We remark that this phase transition is particular to the $X \rightarrow Y$ problem, and is not necessarily present for other control paths $A \rightarrow B$, for arbitrary states A and B .

Nonetheless, the open system solution u demonstrates robustness across a range of D values for other control paths as well. We quantify this by repeating the previous experiment for random Haar target states, and fixed initial state $\psi_0 = |0\rangle$ ($X \rightarrow \text{Haar}$). For each problem, we record the maximum noise value D_{max} for which the fidelity F_{closed} is above 0.98. In Fig. 4 (B), we show the distribution of D_{max} for 100 random Haar states. These results indicate that the QDC algorithm can also be used for computing the optimal controls for unitary dynamics.

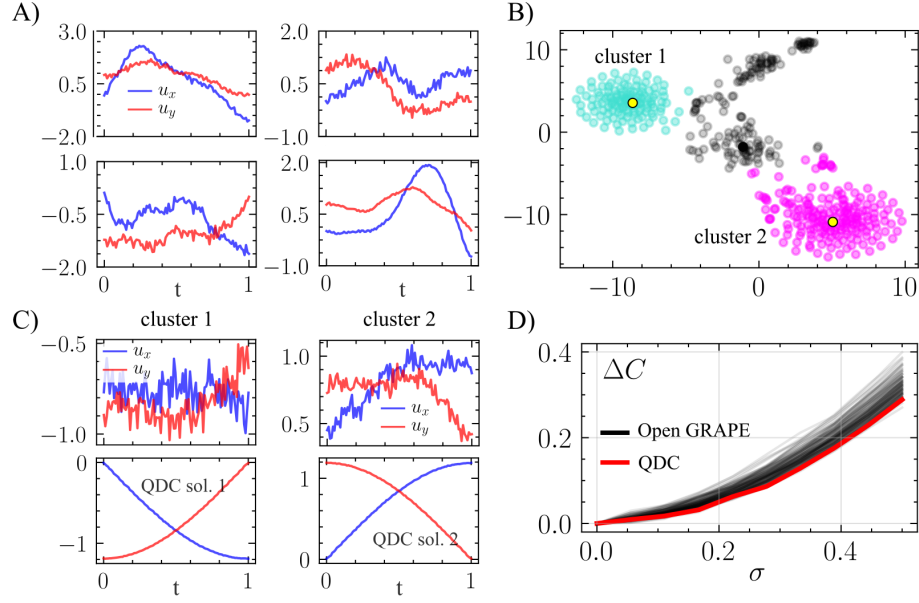


Figure 3: **(A)** Examples of Open GRAPE solutions with diverse levels of regularity for different seeds. **(B)** 2-D t-SNE dimension reduction representation followed by a K-means decomposition of Open GRAPE solutions (red, blue and black dots) and the two average QDC solutions (yellow dots). The cluster of black dots correspond to local minima of relatively high cost C . **(C)** Average Open GRAPE solutions for cluster 1 (red) and cluster 2 (blue). In the bottom panels, the QDC solutions corresponding to each cluster. **(D)** Robustness $\Delta C = C(u + \xi) - C(u)$ versus σ with u the high-fidelity high-ESS QDC solution (red) and the high-fidelity low-ESS Open Grape solution (black).

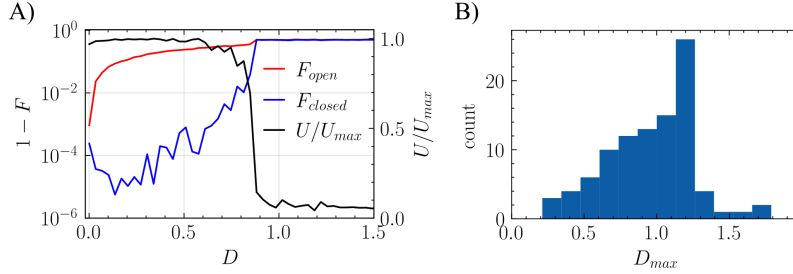


Figure 4: **(A)** Single qubit, $X \rightarrow Y$. In the left y-axis, fidelities F_{open} and F_{closed} vs D ; in the right y-axis, normalized fluence U/U_{max} , vs D , with $U_{max} = 1.86$. Parameters: $T = 1$, $K = 50$, $R = 0.5$, $NT = 100$, $N_{traj} = 2000$ and Q iterates over 5, 50 and 100, and stopping when the fidelity threshold condition $F_{avg} > 0.98$ is met. **(B)** $X \rightarrow Haar$. Distribution of D_{max} for 100 random Haar target states. Average $\langle D_{max} \rangle = 1 \pm 0.3$.

5.3 GHZ states on open NMR systems

In this section, we test the capability of our algorithm in handling systems with multiple qubits. We demonstrate that our QDC algorithm can successfully prepare states for realistic systems such as Nuclear Magnetic Resonance (NMR) molecules. NMR quantum computing has gained significant popularity in recent years as a testbed technology for experimental and theoretical research due to the long coherence times attained compared to the dynamical scales of the system [80]. NMR systems are defined by a total Hamiltonian $H = H_0 + H_c$, where H_0 is the drift and H_c is the control part. The drift and control Hamiltonians are further defined as

$$H_0 = H_Z + H_I \quad H_c = \sum_{n=1}^n u_{ix} \sigma_i^x + u_{iy} \sigma_i^y \quad (26)$$

where $H_Z = \sum_{i=1}^n \pi \nu_i \sigma_i^z$ and $H_I = \sum_{i < j} \frac{\pi}{2} J_{ij} \sigma_i^z \sigma_j^z$. The constants ν_i denote self-energies, commonly called chemical shifts, and J_{ij} are the coupling strengths between the different spins in the system. Pulse-based control is a common approach to control NMR systems. It consists in the sequential application of external radio-frequency pulses across the x - y plane. These pulses are represented by time-dependent fields u_{ia} acting on each qubit i along x and y directions. Configurations like (55) have been proven fully controllable in the sense of state preparation [81], initially rendering NMR systems strong candidates for universal quantum simulators [82].

Due to the typical large difference in magnitude between H_Z and H_I , it is common practice to work in a rotating frame where the dynamics induced by H_Z is absent. Operationally, the rotating frame has the effect of setting $H_Z = 0$ in the drift Hamiltonian H_0 . The optimized pulses in the rotating frame can then easily be transformed back to the laboratory frame. We write the details about this approach in Appendix D.

We write the Lindblad equation for the NMR system as

$$\dot{\rho} = -i[H, \rho] + D \sum_{i=1}^n (\sigma_i^- \rho \sigma_i^+ + \sigma_i^+ \rho \sigma_i^- - \rho) \quad (27)$$

where $H = H_I + H_c$ and dissipation σ_i^\pm of equal strength D acting on individual spins. The control cost is defined as

$$C = -\frac{Q}{2} \left\langle \mathcal{F}(\psi_T) + \frac{R}{2} \int_0^T \left(\sum_{i=1}^n \sum_{a=x,y} u_{ia}^2(t) \right) dt \right\rangle \quad (28)$$

We assume for simplicity, both, $R \rightarrow R/n_c I$ and $D \rightarrow DI$, proportional to the identity matrix I , with constants R, D , respectively, and n_c the number of control components; $n_c = 2n$ for NMR. As in the case of one qubit, we use the transformation (23) to convert the non-Hermitian operators $C_{ia} = \sigma_i^a, a = \pm$ in Eq. (27) into anti-Hermitian operators

$$\tilde{C}_{ib} = C_{ia} A_{ab} \quad \text{for all } i \quad (29)$$

This leads to the following expression for the transformed operators

$$\tilde{C}_{ib} = -i\sigma_i^b \quad \text{for all } i \text{ and } b = x, y. \quad (30)$$

and $\tilde{D} = \frac{1}{2}D$. This transformation leaves the Lindblad equation (27) invariant. The corresponding unraveling is

$$d\psi = -iH_I\psi dt - i \left(\sum_{i=1}^n \sum_{a=x,y} (u_{ia} dt + d\tilde{W}_{ia}) \sigma_i^a \right) \psi - n\tilde{D}\psi dt \quad (31)$$

with $\langle d\tilde{W}_{ia} d\tilde{W}_{jb} \rangle = \delta_{ij} \delta_{ab} \tilde{D} dt$ for $i, j = 1, \dots, n$ and $a, b = x, y$. Equations (28) and (31) define a path integral control problem with $\lambda = \tilde{D}R$. The initial state is $\psi_0 = |0\rangle^2 = Z^2$. We choose the target state ϕ to be a Greenberger-Horne-Zeilinger (GHZ) state, which is defined as $|GHZ_n\rangle := \frac{1}{\sqrt{2}}(|0\rangle^n + |1\rangle^n)$ for n -qubit systems and it represents a maximally entangled state in the global entanglement (or Meyer-Wallach) measure for multipartite systems [83]. In the rotating frame, the target state takes the form $\phi = \frac{1}{\sqrt{2}}(e^{i2\pi\omega T} |0\rangle^n + e^{-i2\pi\omega T} |1\rangle^n)$ with $\omega = \frac{1}{2} \sum_j \nu_j$.

For comparison, we consider the 4-qubit example of [84]. We take the shifts ν_i and couplings J_{ij} from Table I therein. In [84] authors use an iterative version of GRAPE, called i-GRAPE, to optimize the pulses. GRAPE-like methods need, in general, a high number of pulses to validate and find good solutions. As a result, those solutions tend to be very irregular. In addition, the variation is high between solutions for different runs, and the reported solutions for GRAPE and i-GRAPE are very different between each other. In QDC, on the other hand, this is not a constraint and the number of pulses can be arbitrary. Whether the solutions achieve high fidelities or not depends on other factors, such as controllability or the cost parameters. This difference arises from the distinct approach in dealing with time correlations in QDC; we return to this point in Sec. 6.

We prepare a GHZ state for the 4-qubit NMR molecule coupled to an environment. The dynamics corresponds to the Lindblad equation (27). We set the noise coupling $D = 1/T_1$, with T_1 the minimum relaxation time [84]. To compare with the unitary analog in [84], we choose the same final time, $T = 8.8$. In Fig. 5 (A) we show in the main

panel the infidelity $1 - F_{avg}$ reached after convergence for different values of K . In [84], authors report solutions with fidelity 0.9983 with $K = 1760$ GRAPE pulses. In our simulations, we achieve fidelities in the noisy case greater than 0.99 for $K = 5$ pulses (B). These control solutions achieve fidelity greater than 0.9992 in the noiseless case. In Fig. 5 (C) we also show a high rate solution based on $K = 500$ pulses. In this case, the controls are iteratively smoothed during the importance sampling with cubic splines. In the inset of Fig. 5 (A) we show, for the $K = 500$ solution, the infidelity $1 - F_t$, where $F_t = \psi_t^\dagger \phi$, for different trajectories in the time interval.

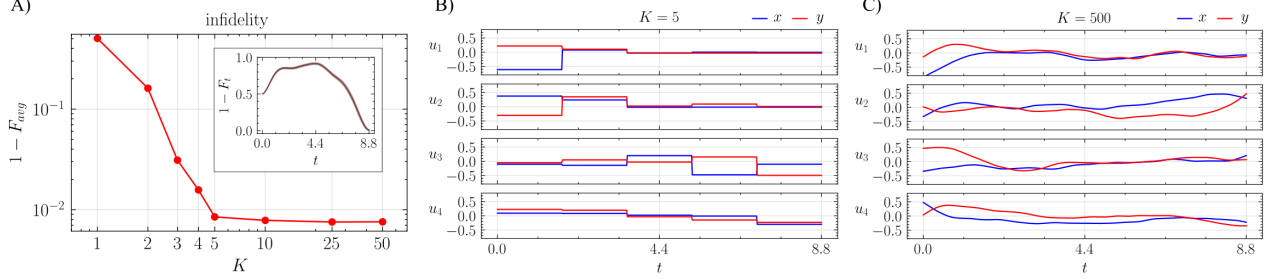


Figure 5: 4-NMR control. (A) In the main panel, the infidelity $1 - F_{avg}$ vs K . In the inset, the infidelity $1 - F_t$ vs time corresponding to a solution with $K = 500$ pulses. (B) Control solutions for $K = 5$ pulses for each qubit. (C) Control solutions for $K = 500$ pulses for each qubit. Parameters: $T = 8.8$, $R = 1$, $Q = 400$, $n_{IS} = 1000$.

5.4 A 10 qubits example

Consider a 1-D spin chain of n qubits with single and pair-wise controls. Since this is a toy model designed to test the scalability of our algorithm for a larger number of qubits, we do not assert its feasibility in a lab setting, but rather emphasize the simplicity of defining such control problems within our framework. For simplicity, we set $H_0 = 0$. The control Hamiltonian is

$$H_c = \sum_{i=1}^n \sum_{a=x,y} u_{ia} \sigma_i^a + \sum_{i=1}^{n-1} \sum_{a,b=x,y} u_{iab} \sigma_i^a \sigma_{i+1}^b \quad (32)$$

where the controls u_{ia} act on spin i , and controls u_{iab} on the pair $i, i + 1$. Note, that H_c is an extension of typical NMR control Hamiltonians [80] with the addition of pair-wise controls.

The open dynamics is described by the Lindblad equation

$$\dot{\rho} = -i[H, \rho] + D_1 \sum_{i=1}^n (\sigma_i^- \rho \sigma_i^+ + \sigma_i^+ \rho \sigma_i^- - \rho) + D_2 \sum_{i=1}^{n-1} \sum_{v,w=\pm} (\sigma_i^v \sigma_{i+1}^w \rho \sigma_i^{-v} \sigma_{i+1}^{-w} - \rho) \quad (33)$$

with dissipation σ^\pm of equal strength D_1 acting on individual spins and with strength D_2 on neighboring pairs of spins.

The control cost is defined as

$$C = \left\langle -\frac{Q}{2} \mathcal{F}(\psi_T) + \frac{1}{2} \int_0^T \left(R_1 \sum_{i=1}^n \sum_{a=x,y} u_{ia}^2 + R_2 \sum_{i=1}^{n-1} \sum_{a,b=x,y} u_{iab}^2 \right) dt \right\rangle \quad (34)$$

Analogous to the previous section, we perform the transformation (23) to map non-Hermitian operators into anti-Hermitian. We transform the operators $C_{ia} = \sigma_i^a, a = \pm$ and $C_{iab} = \sigma_i^a \sigma_{i+1}^b, a, b = \pm$ in Eq. (33) into anti-Hermitian operators

$$\tilde{C}_{ib} = C_{ia} A_{ab} \quad \tilde{C}_{icd} = C_{iab} A_{abcd} \quad \text{for all } i \quad (35)$$

with $A_{abcd} := iA_{ac}A_{bd}$. This leads to the following expression for the transformed operators

$$\tilde{C}_{ib} = -i\sigma_i^b \quad \tilde{C}_{icd} = -i\sigma_i^c \sigma_{i+1}^d \quad \text{for all } i \text{ and } b, c, d = x, y. \quad (36)$$

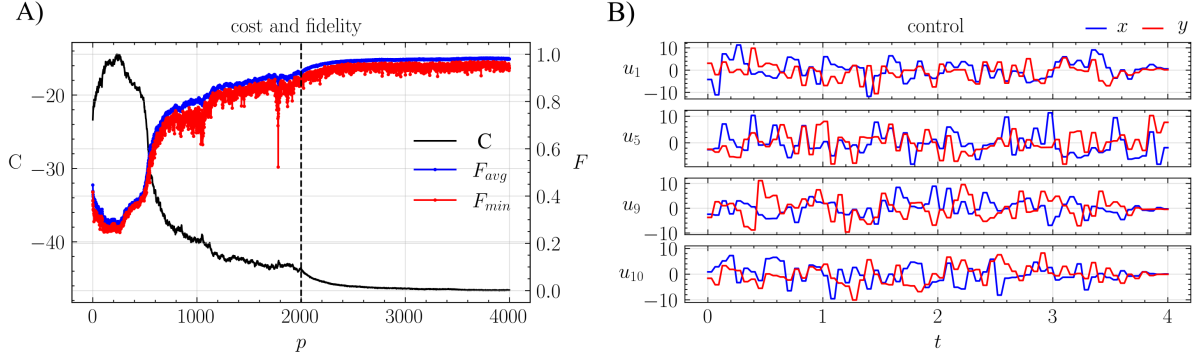


Figure 6: Control of a $n = 10$ qubit 1-D spin chain. The IS training (panel A) has two parts (marked by the vertical dashed line), where in the first part we set the IS window $w = 1$ (no smoothing), and in the second part we change it to $w = 10$. This is to speedup convergence in the first part, and later to improve the statistics. The average fidelity reached $F_{avg} = 0.982 \pm 0.001$. Runtime ~ 6.8 hr on a desktop computer. In panel (B) we illustrate the control solutions for qubits 1, 5, 9 and 10. The x/y components of each control are marked by blue and red colors, respectively. The parameters are $K = 64$, $T = 4$, $R = 0.1$, $D = 0.001$, $Q = 100$, $n_{IS} = 4000$, and $N_{traj} = 100$.

and $\tilde{D}_1 = \frac{1}{2}D_1$, $\tilde{D}_2 = \frac{1}{4}D_2$.

The corresponding unraveling is

$$d\psi = -i \left(\sum_{i=1}^n \sum_{a=x,y} (u_{ia}dt + d\tilde{W}_{ia})\sigma_i^a + \sum_{i=1}^{n-1} \sum_{a,b=x,y} (u_{iab}dt + d\tilde{W}_{iab})\sigma_i^a\sigma_{i+1}^b \right) \psi dt - (n\tilde{D}_1 + 2(n-1)\tilde{D}_2) \psi dt \quad (37)$$

with $\langle d\tilde{W}_{ia}d\tilde{W}_{jb} \rangle = \delta_{ij}\delta_{ab}\tilde{D}_1dt$ for $i, j = 1, \dots, n$ and $a, b = x, y$, and $\langle d\tilde{W}_{iab}d\tilde{W}_{jcd} \rangle = \delta_{ij}\delta_{ac}\delta_{bd}\tilde{D}_2dt$ for $i, j = 1, \dots, n-1$ and $a, b, c, d = x, y$. Equations (34) and (37) define a path integral control problem when

$$\lambda = \tilde{D}_1R_1 = \tilde{D}_2R_2 \quad (38)$$

The initial state is $\psi_0 = |0\rangle^n$. We choose the target state ϕ to be a Greenberger–Horne–Zeilingner (GHZ) state, which is defined as $|GHZ_n\rangle := \frac{1}{\sqrt{2}}(|0\rangle^n + |1\rangle^n)$ for n -qubit systems and it represents a maximally entangled state in the global entanglement (or Meyer–Wallach) measure for multipartite systems [83]. We set $R_1 = R_2 = R/n_c$ with $n_c = 2n + 4(n-1)$ the total number of controls. This normalization defines a fluence cost per unit control. The PI condition (38) then implies that $\tilde{D}_2 = \tilde{D}_1$ or $D_2 = 2D_1$. We take as free parameters R and D_1 . We run the algorithm for $n = 10$ qubits. The results are shown in Fig. 6, showing the usefulness of QDC for relatively large systems. Note, a direct implementation of this problem in Open GRAPE would require to compute and store matrix exponentials of size $N^2 \times N^2$ at each step K , which is memory intensive and requires an efficient implementation of the algorithm (see for example [27, 85]) and/or dedicated software. Our QDC algorithm runs in a desktop computer.

6 Discussion

The main features of our method can be summarized as follows: 1) it is *state-centered*: the quantum trajectories are obtained by propagating state vectors of size N , opposed to most common density-based approaches, which require density matrices of size N^2 ; in this way, our algorithm inherently comprises a quadratic advantage in runtime over density-based methods, such as the PMP method or the adjoint method [29]. 2) it is *embarrassingly parallel*: The core of QDC computation is to learn a model on the basis of self-generated data (sample trajectories) and this procedure is iterated using improved controls until convergence. The importance sampling updates Eqs. (14) and (16) can be very efficiently parallelized by noting that the gradient consists of a sum over the data and that the computation of this sum can be distributed over m machines so that the updated parameters $\theta_{p+1} = \theta_p + \frac{1}{m} \sum_{i=1}^m d\theta_p^{(i)}$ with $d\theta_p^{(i)}$ the gradient update computed on machine i . No large volumes of simulated raw data

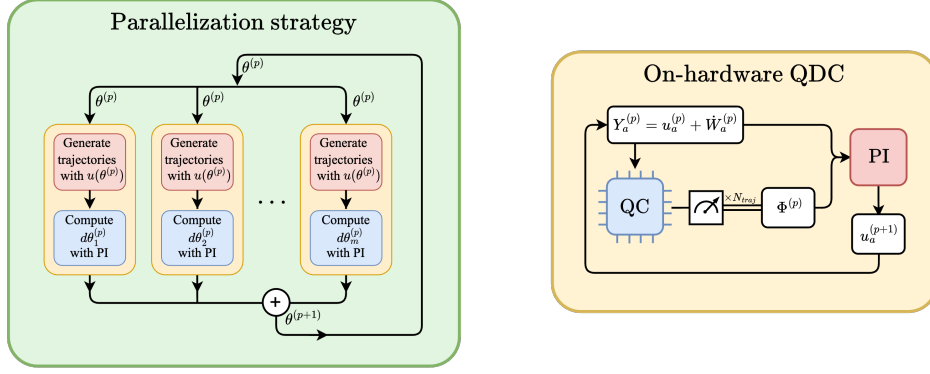


Figure 7: **(Left)** During each iteration, samples are generated using control functions $u(\theta^{(p)})$. These samples are used to compute new parameters $\theta^{(p+1)}$. These two steps can be distributed on many machines with minimal communication overhead, since no large volumes of simulated raw data need to be transferred between machines, only the parameter updates. **(Right)** At each IS step p , simulate in the quantum computer (QC) N_{traj} unitary trajectories with input control signal $Y_a^{(p)} = u_a^{(p)} + \dot{W}_a^{(p)}$, where $u_a^{(p)}$ is the control trajectory and $\dot{W}_a^{(p)}$ are the N_{traj} self-generated noise trajectories. At time T , measure the state and produce N_{traj} measurements $\Phi^{(p)} = \psi_T^{(p)\dagger} H_{\text{target}} \psi_T^{(p)}$. Input the current control, the noise trajectories and the measurements into the IS formula (17) and update the control to $u_a^{(p+1)}$. Repeat.

need to be transferred between machines, only the parameter updates. See Fig. 7 (A). This results in close-to-linear speedup. 3) An important point concerns the nature of control computation in QDC. For any control problem, the primary computational challenge is to account for how early control actions influence the system’s state and cost at later times. For instance, GRAPE and PMP use some form of backward evolution of the co-state to estimate this dependence. QDC, instead, uses an entirely different mechanism, by generating forward sampled stochastic particle trajectories that are weighted with their exponentiated control cost. These global statistics are then used to update the parameters in each time bin independently. This is a prominent feature of our QDC algorithm and stands out from other methods where a direct access to the objective gradients is needed. Our experiments suggest that this is may represent a more effective way to compute the optimal control, when the control problem is of the PI form.

6.1 A proposal for on-hardware QDC

The QDC algorithm includes a subroutine for simulating quantum trajectories of the stochastic dynamics described by (20), and this scales exponentially on classical hardware. Other QOC approaches suffer from the same curse, for which replacing classical simulation by quantum hardware implementations seems not only favorable for better scaling but necessary. Here, we propose a way to run the QDC framework on quantum hardware. The following can be seen as a realization of a quantum-classical optimization protocol [86], where the optimization part is achieved by PI control. The crucial observation is that the stochastic dynamics dictated by (20) can be interpreted as a random unitary dynamics [78]. This dynamics is defined by a Hamiltonian $H = H_0 + H_c$, where $H_c = Y_a H_a$ is determined by a random control signal $Y_a = u_a + \dot{W}_a$, composed by a deterministic part u_a , and a stochastic part \dot{W}_a —the time derivative of the Wiener process is formal, and should be interpreted in the discrete sense. Given a suitable time discretization dt , we can replace the subroutine with the classical simulations of the open dynamics (20) by simulations on the actual quantum hardware.

In Fig. 7, we show a flow diagram illustrating the on-hardware QDC algorithm’s operation for a general end cost $\Phi(\psi_T) = \psi_T^\dagger H_{\text{target}} \psi_T$, with H_{target} an arbitrary Hermitian matrix. The algorithm’s fundamental operation involves iterative state preparations and measurements to optimize the quantum dynamics. The computational complexity, in terms of required re-preparations and measurements, follows a scaling $\propto \frac{\alpha}{\varepsilon_q^2 \varepsilon_c^2}$ [86]. Here, $\alpha = \mathcal{O}(\text{poly}(n))$ with n the system’s size, and ε_q and ε_c denote the precision requirements for quantum and classical expectation value estimations, respectively, in the on-hardware QDC loop. This naive scaling can be substantially improved through better estimation techniques and the parallelization strategies discussed earlier.

We remark that the on-hardware implementation of QDC can be realized either, at the circuit level, or pulse level. In the first, the optimization targets parametrized quantum gates encoding the quantum dynamics. The control parameters are the gate parameters within the quantum circuit. Variational quantum algorithms (VQAs) operate in this level. The pulse level operates below the circuit level, and involves direct optimization of the Hamiltonian dynamics through successive applications of electromagnetic pulses, analogous to the NMR control described in Sec. 5.3. Here, the control parameters are the actual physical fields driving the quantum system. Methods for commuting between these two levels have been extensively studied [87], establishing the circuit level as a well-defined abstraction layer above the physical pulse level [86].

Pulse-based control may offer several potential advantages over circuit-based control. For instance, on four transmon qubits, a reduction in state preparation time of roughly three orders of magnitude compared to gate based strategies was demonstrated [88]. More recently, authors [89] have recently applied pulse-based optimal control for ground state preparation, demonstrating that pulse-based control required less time than an equivalent digital circuit. These approaches restrict to closed quantum systems and open loop control. The QDC method provides a realistic and computationally tractable approach to extend this work in the direction of open quantum systems and feedback control. A comprehensive analysis comparing QDC performance with state-of-the-art variational quantum algorithms [88, 89], including detailed benchmarking results, will be addressed in future work.

7 Conclusion and Outlook

In this work we propose Quantum Diffusion Control (QDC), a novel approach for optimal control of open quantum systems. We bring together tools from path integral control and quantum trajectories to frame a broad class of quantum control problems in the language of stochastic optimal control theory. Stochastic optimal control problems usually demand the integration of a Hamilton-Jacobi-Bellman equation, which is prohibitive for large systems. QDC bypasses this requirement giving the optimal solution explicitly as a path integral. Optimal controls are then computed by sampling stochastic trajectories in the Hilbert space. The path integral formulation of the control problem unlocks the possibility of integrating Monte Carlo and Machine Learning techniques directly into the estimation process. Here, we use iterative importance sampling, a scheme where the controls are incrementally improved and the optimal control solutions are seen as fixed points of this process. For linear parametrizations, either open-loop or feedback, the importance sampling updates are computed as stochastic averages, as given by Eqs. (14) and (16). For non-linear parametrizations –e.g., when the control functions $u(\theta)$ are represented by deep neural networks –a more general iterative importance sampling algorithm is given by the Path integral Cross-Entropy (PICE) method [90], involving the gradients $\partial u / \partial \theta$. As in any neural network training, these gradients can be computed using automatic differentiation [91].

The QDC algorithm, including the importance sampling method and their generalization to PICE, automatically generalize to compute feedback control solutions. However, these solutions require information about the quantum state through measurement. Since the quantum state is only partially observable through measurement, the control problem becomes what is known as a *partial observable control problem* [60]. A compromise between information gain and minimal disruption of the quantum state is given by the so-called *weak or continuous measurement* [61, 62, 63]. The extension of our approach to incorporate partial observation and continuous measurements is currently under development and will be presented in future work.

A Unraveling calculations

Proof. Proof of Proposition 1. Consider the stochastic dynamics

$$d\psi = -iH'\psi dt - \frac{1}{2}D_{ab}C_b'^\dagger C_a'\psi dt + C_a'\psi dW^a \quad (39)$$

with $\langle dW_a dW_b \rangle = D_{ab}dt$ and H', C' to be defined later. Define the quantum state $P = \psi\psi^\dagger$. Then using Ito calculus, the dynamics of P is

$$dP = d\psi\psi^\dagger + \psi d\psi^\dagger + d\psi d\psi^\dagger = -i[H', P]dt + \mathcal{D}[C', D](P)dt + [C_a'PdW_a + \text{h.c.}] \quad (40)$$

ψ is a stochastic vector with norm $\|\psi\|^2 = \psi^\dagger\psi$. Using Ito calculus, the change in the norm is given by

$$d(\|\psi\|^2) = d\psi^\dagger\psi + \psi^\dagger d\psi + d\psi^\dagger d\psi = \psi^\dagger(C_a' + (C_a')^\dagger)\psi dW_a \quad (41)$$

We can ensure that $\|\psi\|^2$ is conserved by defining $C_a' = C_a - c_a$ with $c_a = \psi^\dagger C_a^{(h)}\psi$ and $C_a^{(h)}$ the Hermitian part of C_a . Note, that c_a is real. With this choice Eqs. (39) and (40) become⁵

$$d\psi = -iH'\psi dt - \frac{1}{2}D_{ab}(C_b - c_b)^\dagger(C_a - c_a)\psi dt + (C_a - c_a)\psi dW_a \quad (42)$$

$$dP = -i[H' - iD_{ab}c_a C_b^{(ah)}, P] + \mathcal{D}[C, D](P)dt + [(C_a - c_a)PdW_a + \text{h.c.}] \quad (43)$$

with $C_a^{(ah)} = \frac{1}{2}(C_a - C_a^\dagger)$. To connect to the Lindblad equation, define $H = H' - iD_{ab}c_a C_b^{(ah)}$. Then substitution in (42) and (43) yields (2) and

$$dP = -i[H, P]dt + \mathcal{D}[C, D](P)dt + [(C_a - c_a)PdW_a + \text{h.c.}] \quad (44)$$

Define $\rho := \langle P \rangle$ and $\langle dP \rangle := \rho dt$. Taking the average of (44) yields the Lindblad equation (1), which completes the proof. \square

B Path integral control theory

In this section we describe some basic results regarding PI control theory. For further details the reader may consult the original papers [92, 93].

Define

$$\psi(t, x) = e^{-J(t, x)/\lambda} \quad \phi(t) = e^{(S^u(t) - S^u(t_0))/\lambda}$$

where $\lambda I = R\nu$. Furthermore we define the stochastic processes $\psi(t) = \psi(t, X_t^u)$, $u(t) = u(t, X_t^u)$ and $u^*(t) = u^*(t, X_t^u)$

Lemma 1. For all t in $t_0 \leq t \leq t_1$

$$e^{-S^u(t)/\lambda} - \psi(t) = \frac{1}{\lambda\phi(t)} \int_t^{t_1} \phi(s)\psi(s)(u^*(s) - u(s))^T R dW_s \quad (45)$$

⁵

$$\begin{aligned} \mathcal{D}[C', D](P) &= D_{ab} \left((C_a - c_a)P(C_b - c_b)^\dagger - \frac{1}{2}\{(C_b - c_b)^\dagger(C_a - c_a), P\} \right) \\ &= \mathcal{D}[C, D](P) + \frac{1}{2}D_{ab}c_a[C_b^\dagger, P] - \frac{1}{2}D_{ab}c_a[C_b, P] \\ &= \mathcal{D}[C, D](P) - D_{ab}c_a[C_b^{(ah)}, P] = \mathcal{D}[C, D](P) - i[-iD_{k\ell}c_k C_\ell^{(ah)}, P] \end{aligned}$$

Proof. Define the optimal cost-to-go as the minimal expected cost starting in any x at time t with $t_0 \leq t \leq t_1$

$$J(t, x) = \min_u \langle S^u(t) \rangle_{X_t^u=x} \quad u^*(t, x) = \operatorname{argmin}_u \langle S^u(t) \rangle_{X_t^u=x} \quad (46)$$

where the minimization is over all smooth functions $u(\cdot, s), t \leq s \leq t_1$. The HJB equation for the control problem Eqs. (6) and (7) is

$$-J_t = \min_u \left(V + \frac{1}{2} u^T R u + (f + g u)^T J_x + \frac{1}{2} \operatorname{Tr}(g \nu g^T J_{xx}) \right)$$

where subscripts t, x denote differentiation with respect to t, x and with boundary condition $J(t_1, x) = \Phi(x)$. We can solve for u , which gives $u^* = -R^{-1} g^T J_x$ and

$$-J_t = V - \frac{1}{2} J_x^T g R^{-1} g^T J_x + f^T J_x + \frac{1}{2} \operatorname{Tr}(g \nu g^T J_{xx}) \quad (47)$$

We assume that the matrices R, ν are related such that $R = \lambda \nu^{-1}$ with $\lambda > 0$. In terms of ψ , Eq. (47) becomes linear

$$\psi_t + f^T \psi_x + \frac{1}{2} \operatorname{Tr}(g \nu g^T \psi_{xx}) = \frac{V}{\lambda} \psi \quad (48)$$

Alternatively, we consider the stochastic process $\psi(t) = \psi(t, X_t^u)$. Using \hat{I} to calculus we obtain

$$d\psi = \left(\psi_t + \psi_x^T (f + g u) + \frac{1}{2} \operatorname{Tr}(g \nu g^T \psi_{xx}) \right) dt + \psi_x^T g dW = \frac{V}{\lambda} \psi + \psi_x^T g (u dt + dW)$$

where we used Eq. (48), with boundary condition $\psi(t_1, x) = e^{-\Phi(x)/\lambda}$. Using the definition of $\phi(t)$ we obtain

$$d\phi = -\frac{1}{\lambda} (V dt + u^T R dW)$$

with initial condition $\phi(t_0) = 1$. Using the product rule we obtain

$$d(\phi\psi) = d\phi\psi + \phi d\psi + d[\phi, \psi] = -\frac{1}{\lambda} \psi \phi u^T R dW + \phi \psi_x^T g dW = \frac{1}{\lambda} \phi \psi (u^* - u)^T R dW$$

where in the last step we used $u^* = \lambda R^{-1} g^T \frac{\psi_x}{\psi}$. Integrating from t to t_1 we obtain

$$\phi(t_1)\psi(t_1) - \phi(t)\psi(t) = \frac{1}{\lambda} \int_t^{t_1} \phi(s)\psi(s)(u^*(s) - u(s))^T R dW_s$$

We use $\phi(t_1) = \phi(t) e^{(S^u(t_1) - S^u(t))/\lambda}$ and divide by $\phi(t)$ to obtain Eq. (45). \square

Corollary 2. We take the expectation of Eq. (45) with respect to $dW_{t:t_1}$ and condition on events up to time t , which we call a filtration \mathcal{F}_t , we obtain

$$\psi(t) = \left\langle e^{-S^u(t)/\lambda} \right\rangle_{\mathcal{F}_t} \quad (49)$$

The following path integral control theorem is useful to estimate these parameters for all times from one set of samples $X_{t_0:t_1}^u$.

Theorem 3. Let $f : \mathbb{R} \times \mathbb{R}^n \rightarrow \mathbb{R}$ and define the process $f_t = f(t, X_t^u)$. Then

$$\left\langle e^{-S^u(t_0)/\lambda} \int_{t_0}^{t_1} (u^*(s) - u(s)) f(s) ds \right\rangle = \left\langle e^{-S^u(t_0)/\lambda} \int_{t_0}^{t_1} f(s) dW_s \right\rangle \quad (50)$$

where the expectation is with respect to the stochastic process (6).

Proof. Consider Lemma (45) for $t = t_0$. Multiply both sides by $\int_{t_0}^{t_1} f(s) dW_s$ and take the expectation value

$$\left\langle e^{-S^u(t_0)} \int_{t_0}^{t_1} f(s) dW_s \right\rangle = \left\langle \int_{t_0}^{t_1} f(s) dW_s \int_{t_0}^{t_1} \phi(s') \psi(s') (u^*(s') - u(s'))^T \frac{R}{\lambda} dW_{s'} \right\rangle \quad (51)$$

Using $RD = \lambda$ and Ito isometry we have

$$\left\langle e^{-S^u(t_0)} \int_{t_0}^{t_1} f(s) dW_s \right\rangle = \int_{t_0}^{t_1} \langle f(s) \phi(s) \psi(s) (u^*(s) - u(s)) \rangle ds \quad (52)$$

Using the definition of $\psi(s)$ and $\phi(s)$ we write

$$\left\langle e^{-S^u(t_0)} \int_{t_0}^{t_1} f(s) dW_s \right\rangle = \int_{t_0}^{t_1} \left\langle f(s) e^{(S^u(s) - S^u(t_0))/\lambda} \left\langle e^{-S^u(t_0)} \right\rangle_{\mathcal{F}_s} (u^*(s) - u(s)) \right\rangle ds \quad (53)$$

Finally, by applying the law of total expectation we obtain (50). \square

Corollary 4. By setting $f(t) = \delta_{t \in I}$ with $I = [t_0, t_0 + dt]$, diving by dt and taking the limit $dt \rightarrow 0$ we establish the proof of (10).

C Open GRAPE

Here we summarize the details of our implementation of Open GRAPE for the benchmarking part of Section 5.1. For further details concerning the definition of Open GRAPE algorithm we refer the reader to [27]. Given the cost objective (18) and the control model Eq. (12) with R a positive scalar, the first order Open GRAPE update rule (ignoring terms of $\mathcal{O}(dt^2)$ and higher) becomes

$$A_{ak} \rightarrow A'_{ak} = A_{ak} - \varepsilon \frac{\partial C}{\partial A_{ak}}$$

with

$$\frac{\partial C}{\partial A_{ak}} = \frac{iQ}{2} \text{Tr}(\lambda_k [H_a, \rho_k]) dt + R A_{ak} dt$$

where ρ_k is the forward-propagated state from ρ_0 to time t_k and λ_k is the backward-propagated state from ρ_{target} to time t_k , ε is the learning rate, and dt is the time step. We implement the algorithm in Python language. For the dynamics simulation of the backward and forward propagations we use the open-source Python package `dynamics` [94].

The learning rate ε usually needs to be carefully chosen in order to avoid overshooting. In the case of GRAPE for closed systems, work [95] reported an adaptive learning rate at each j step of ε/j^α with $\alpha = 1/2$ was enough to avoid overshooting of local minima/saddle points. We found this approach not suitable for our benchmarking purposes as it required an excessive fine tuning of α for different types of seeds. We choose instead the following protocol: every time the cost $C(A') \geq C(A)$, where A the current solution and A' the new solution, the learning rate is reduced by a factor 10 and $C(A')$ is recomputed until either $C(A') < C(A)$ or ε is reduced a maximum number of times that we set to 10. This stopping condition allows us to capture local minima and detect when the first order approximation of the gradient update starts to fail. At the start of each run, we sample random seeds u from Gaussian distributions (centered at zero, 1, and -1, with standard deviation 2) and uniform distributions (integers between -10 and 10, with a scale factor of 1 and 0.5).

D Open NMR control theory

D.1 Rotating frame transformation

Define the unitary transformation

$$U = \exp(iH_Z t) \quad H_Z = \pi \sum_j \nu_j \sigma_j^z \quad (54)$$

It represents a transformation from the lab frame to a multiple rotating frame. Given the state ρ in the lab frame, define the transformed state to the rotating frame by $\rho' = U\rho U^\dagger$. Assume ρ follows the generic Lindblad equation

$$\dot{\rho} = -i[H_Z + H_I + H_c, \rho] + \mathcal{D}[D, J]\rho \quad (55)$$

where, for simplicity, D is a real scalar and the J_a are arbitrary dissipators.

Lemma 2. *The transformed state ρ' follows the Lindblad equation*

$$\dot{\rho}' = -i[H_I + H'_c, \rho'] + \mathcal{D}[D, J']\rho' \quad (56)$$

where

$$H'_c = \sum_i u'_{ix} \sigma_i^x + u'_{iy} \sigma_i^y \quad J'_a = U J_a U^\dagger \quad (57)$$

and the controls in the rotating frame, $u'_i = (u'_{ix}, u'_{iy})^T$, are related to those in the lab frame, $u_i = (u_{ix}, u_{iy})^T$, by a real rotation

$$u'_i = S_i(t) u_i \quad S_i(t) = \begin{pmatrix} \cos(2\pi\nu_i t) & \sin(2\pi\nu_i t) \\ -\sin(2\pi\nu_i t) & \cos(2\pi\nu_i t) \end{pmatrix} \quad (58)$$

Proof. By differentiating ρ' w.r.t. time we obtain

$$\begin{aligned} \dot{\rho}' &= \dot{U} \rho U^\dagger + U \dot{\rho} U^\dagger + U \rho \dot{U}^\dagger \\ &= -i[H_I + H'_c, \rho'] + \mathcal{D}[D, J']\rho' \end{aligned}$$

where $H'_c = U H_c U^\dagger$ and $J'_a = U J_a U^\dagger$.

Next, compute

$$H'_c = U H_c U^\dagger = \sum_i u_{ix} (U \sigma_i^x U^\dagger + u_{iy} U \sigma_i^y U^\dagger)$$

For each spin i we obtain

$$\begin{aligned} U \sigma_i^x U^\dagger &= e^{i\pi\nu_i t \sigma_i^z} \sigma_i^x e^{-i\pi\nu_i t \sigma_i^z} \\ &= \cos(2\pi\nu_i t) \sigma_i^x - \sin(2\pi\nu_i t) \sigma_i^y \end{aligned}$$

and

$$\begin{aligned} U \sigma_i^y U^\dagger &= e^{i\pi\nu_i t \sigma_i^z} \sigma_i^y e^{-i\pi\nu_i t \sigma_i^z} \\ &= \cos(2\pi\nu_i t) \sigma_i^y + \sin(2\pi\nu_i t) \sigma_i^x \end{aligned}$$

Then, we can write H'_c as

$$H'_c = \sum_i u'_{ix} \sigma_i^x + u'_{iy} \sigma_i^y$$

where

$$\begin{aligned} u'_{ix} &= \cos(2\pi\nu_i t) u_{ix} + \sin(2\pi\nu_i t) u_{iy} \\ u'_{iy} &= -\sin(2\pi\nu_i t) u_{ix} + \cos(2\pi\nu_i t) u_{iy} \end{aligned} \quad (59)$$

By defining

$$S_i(t) = \begin{pmatrix} \cos(2\pi\nu_i t) & \sin(2\pi\nu_i t) \\ -\sin(2\pi\nu_i t) & \cos(2\pi\nu_i t) \end{pmatrix}, \quad (60)$$

$u'_i = (u'_{ix}, u'_{iy})^T$ and $u_i = (u_{ix}, u_{iy})^T$, we rewrite (59) as $u'_i = S_i(t) u_i$ and the Lemma is proved. \square

Assume the NMR system is in interaction with a EM field bath, which we encode in the dissipators $C_a = \sigma_i^+, \sigma_i^-$ ($i = 1, \dots, n$).

Lemma 3. *The dissipator in (55) is invariant under the action of U , i.e. $\mathcal{D}[D, C'] = \mathcal{D}[D, C]$.*

Proof. Apply the unitary transformation U to the Lindblad operators.

$$\begin{aligned} U\sigma_i^+U^\dagger &= e^{i\pi\nu_i t\sigma_i^z}\sigma_i^+e^{-i\pi\nu_i t\sigma_i^z} \\ &= e^{i2\pi\nu_i t}\sigma_i^+ \end{aligned}$$

where we used that $[\sigma_i^z, \sigma_i^+] = 2\sigma_i^+$. Analogously for σ_i^- , we have $U\sigma_i^-U^\dagger = e^{-i2\pi\nu_i t}\sigma_i^-$. Therefore, the Lindblad operators C'_a in the rotating frame are the same as in the lab frame up to phase factors. As the dissipator is invariant under phase transformations, the Lemma is thus proven. \square

D.2 Control problem equivalence

The main purpose of the unitary transformation U is to factor out potentially fast frequencies ν from the definition of the control problem that are not necessary for computing the optimal control and may even hinder the efficient search for a solution. By defining and solving the control problem in the rotating frame, we can uniquely map the optimal solution back to the lab frame through the action of the unitary transformation in control space. In this Section we describe a general invariance present in the control problem under certain family of transformations \mathcal{T} .

Assume the Lindblad equation for an open NMR system

$$\dot{\rho} = -i[H, \rho] + \mathcal{D}[D, C]\rho \quad (61)$$

with $H = H_Z + H_I + H_c$ and dissipator

$$\mathcal{D}[D, C]\rho = \sum_j D_{jab} \left(C_{ja}\rho C_{jb}^\dagger - \frac{1}{2}\{C_{jb}^\dagger C_{ja}, \rho\} \right).$$

where index j labels qubit j , and the dissipation operators C_{ja} act on qubit j . The noise matrix D is in block diagonal form $D := \bigoplus_j D_j$ with $(D_j)_{ab} = D_{jab}$.

Define the cost

$$C[x] = -\frac{Q}{2}\text{Tr}(\rho_T \rho_{tar}) + \frac{1}{2} \sum_j \int_0^T u_j^T R_j u_j dt \quad (62)$$

where the tuple $x := (\rho_T, \rho_{tar}, u, R)$ with $R := \bigoplus_j R_j$ block diagonal.

Consider U as in Section D.1, and define the transformation $\mathcal{T} = (U, S)$ to the rotating frame by it's action on pair (ρ, u) , with $u = u_i$ ($i = 1, \dots, n$), as $\mathcal{T}(\rho, u) = (U\rho U^\dagger, Su)$, and it's action on pair (D, R) as $\mathcal{T}(D, R) = (S^T D S, S^T R S)$.

Under \mathcal{T} , the dissipators C_{ja} transform as

$$UC_{ja}U^\dagger = e^{i\alpha_j} \sum_b S_{jab} C_{jb} \quad (63)$$

where S_j ($j = 1, \dots, n$) is an orthogonal matrix with $S_j S_j^T = 1$, α_j arbitrary real numbers, and define $S = \bigoplus_j S_j$.

Lemma 4. *The dissipator $\mathcal{D}[D, C]$ is invariant under \mathcal{T} , i.e. $\mathcal{D}[D', C'] = \mathcal{D}[D, C]$.*

Proof. The results follows by applying $\mathcal{T}D = SDS^T$ and definition (63) to the dissipators C_{ja} . \square

Theorem 5. *The cost $C[x]$ in (62) is invariant under \mathcal{T} and the optimal control solutions u'^* and u^* in the rotating and lab frames, respectively, are related by $u'^* = Su^*$.*

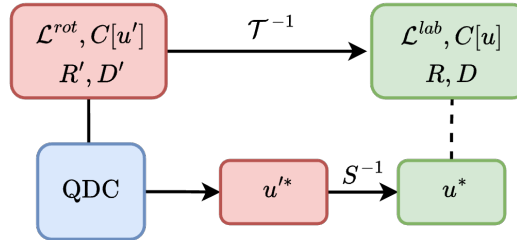
Proof. Write the action of \mathcal{T} on C as

$$\begin{aligned}
(\mathcal{T}C)[x] &= C[\mathcal{T}x] \\
&= -\frac{Q}{2}\text{Tr}(\rho'_T \rho'_{tar}) + \frac{1}{2} \sum_j \int_0^T u'_j{}^T R'_j u'_j dt \\
&= -\frac{Q}{2}\text{Tr}(U \rho_T U^\dagger U \rho_{tar} U^\dagger) + \frac{1}{2} \sum_j \int_0^T (Su_j)^T S R_j S^T (Su_j) dt \\
&= C[x]
\end{aligned}$$

where in the last line we used the unitarity/orthogonality of U and S_i , respectively. Thus, $C[x] = C[x']$ and the invariance of C follows.

Next, fix ρ_{tar} and R , and consider the optimal solution in the lab frame $u^* = \text{argmin}_u C[u]$, which satisfies $C[u^*] \leq C[u] \forall u$. By invariance of C under \mathcal{T} , and given that \mathcal{T} is invertible, the transformation Su^* satisfies $C[Su^*] \leq C[u'] \forall u'$ where $u' = Su$. Thus, the optimal solution in the rotating frame u'^* corresponds to a rotation of the optimal solution in the lab frame, $u'^* = Su^*$. \square

Provided that the dissipators C' in the rotating frame can be transformed to anti-Hermitian operators, we can solve the control problem in the rotating frame using the QDC algorithm. By virtue of Theorem 5, The optimal control u'^* in the rotating frame can be mapped back to the lab frame. The following diagram illustrates the end-to-end workflow.



where \mathcal{L}^{rot} , \mathcal{L}^{lab} are the Lindbladian operators in the rotating and lab frames, respectively.

Example 1. A particular example of \mathcal{T} is the case in which the dissipators $C_a = \sigma_i^+, \sigma_i^-$. Then, S corresponds to the rotation defined in (58) and we can use the transformation A defined in (23) to transform to anti-hermitian operators and simulate the problem using QDC.

Example 2. When the target state in the lab frame is a GHZ state, i.e. $\phi = |GHZ\rangle$, the corresponding state in the rotating frame becomes $\phi' = U_T |GHZ\rangle = \frac{1}{\sqrt{2}}(e^{i2\pi\omega T} |0\rangle^n + e^{-i2\pi\omega T} |1\rangle^n)$ with $\omega = \frac{1}{2} \sum_j \nu_j$. In particular, note that $\phi' = \phi$ whenever $\omega T \in \mathbb{Z}$.

References

- [1] Lidar, D. A. & Brun, T. A. *Quantum error correction* (Cambridge university press, 2013).
- [2] Georgescu, I. M., Ashhab, S. & Nori, F. Quantum simulation. *Reviews of Modern Physics* **86**, 153–185 (2014).
- [3] Giovannetti, V., Lloyd, S. & Maccone, L. Advances in quantum metrology. *Nature photonics* **5**, 222–229 (2011).
- [4] Degen, C. L., Reinhard, F. & Cappellaro, P. Quantum sensing. *Reviews of modern physics* **89**, 035002 (2017).
- [5] Arrazola, J. M. *et al.* Quantum circuits with many photons on a programmable nanophotonic chip. *Nature* **591**, 54–60 (2021).

- [6] Hermans, S. *et al.* Qubit teleportation between non-neighbouring nodes in a quantum network. *Nature* **605**, 663–668 (2022).
- [7] Baßler, P. *et al.* Synthesis of and compilation with time-optimal multi-qubit gates. *Quantum* **7**, 984 (2023).
- [8] Bushev, P. *et al.* Feedback Cooling of a Single Trapped Ion. *Physical Review Letters* **96**, 043003 (2006). URL <https://link.aps.org/doi/10.1103/PhysRevLett.96.043003>.
- [9] Rossi, M., Mason, D., Chen, J., Tsaturyan, Y. & Schliesser, A. Measurement-based quantum control of mechanical motion. *Nature* **563**, 53–58 (2018). URL <https://www.nature.com/articles/s41586-018-0643-8>. Publisher: Nature Publishing Group.
- [10] Adams, C. S., Pritchard, J. D. & Shaffer, J. P. Rydberg atom quantum technologies. *Journal of Physics B: Atomic, Molecular and Optical Physics* **53**, 012002 (2019).
- [11] Henriet, L. *et al.* Quantum computing with neutral atoms. *Quantum* **4**, 327 (2020).
- [12] Magrini, L. *et al.* Real-time optimal quantum control of mechanical motion at room temperature. *Nature* **595**, 373–377 (2021). URL <https://www.nature.com/articles/s41586-021-03602-3>. Publisher: Nature Publishing Group.
- [13] Glaser, S. J. *et al.* Training Schrödinger’s cat: Quantum optimal control: Strategic report on current status, visions and goals for research in Europe. *The European Physical Journal D* **69**, 279 (2015). URL <http://link.springer.com/10.1140/epjd/e2015-60464-1>.
- [14] Koch, C. P. *et al.* Quantum optimal control in quantum technologies. Strategic report on current status, visions and goals for research in Europe. *EPJ Quantum Technology* **9**, 19 (2022). URL <https://epjquantumtechnology.springeropen.com/articles/10.1140/epjqt/s40507-022-00138-x>.
- [15] Cong, S. *Control of quantum systems: theory and methods* (John Wiley & Sons, 2014).
- [16] d’Alessandro, D. *Introduction to quantum control and dynamics* (Chapman and hall/CRC, 2021).
- [17] Mahesh, T., Batra, P. & Ram, M. H. Quantum optimal control: Practical aspects and diverse methods. *Journal of the Indian Institute of Science* **103**, 591–607 (2023).
- [18] Khaneja, N., Reiss, T., Kehlet, C., Schulte-Herbrüggen, T. & Glaser, S. J. Optimal control of coupled spin dynamics: design of nmr pulse sequences by gradient ascent algorithms. *Journal of magnetic resonance* **172**, 296–305 (2005).
- [19] Chen, Y. *et al.* Accelerating quantum optimal control through iterative gradient-ascent pulse engineering. *Physical Review A* **108**, 052603 (2023). URL <https://link.aps.org/doi/10.1103/PhysRevA.108.052603>. Publisher: American Physical Society.
- [20] Caneva, T., Calarco, T. & Montangero, S. Chopped random-basis quantum optimization. *Physical Review A* **84**, 022326 (2011).
- [21] Krotov, V. F. Global methods in optimal control theory. In *Advances in nonlinear dynamics and control: a report from Russia*, 74–121 (Springer, 1996).
- [22] Tannor, D., Kazakov, V., Orlov, V., Broeckhove, J. & Lathouwers, L. Time-dependent quantum molecular dynamics. *Nato ASI Series B* **299**, 347 (1992).
- [23] Reich, D. M., Ndong, M. & Koch, C. P. Monotonically convergent optimization in quantum control using krotov’s method. *The Journal of chemical physics* **136** (2012).
- [24] Abdelhafez, M., Schuster, D. I. & Koch, J. Gradient-based optimal control of open quantum systems using quantum trajectories and automatic differentiation. *Physical Review A* **99**, 1–20 (2019). 1901.05541.
- [25] Boscain, U., Sigalotti, M. & Sugny, D. Introduction to the Pontryagin Maximum Principle for Quantum Optimal Control. *PRX Quantum* **2**, 030203 (2021). URL <http://arxiv.org/abs/2010.09368>. 2010.09368.

- [26] Koch, C. P. Controlling open quantum systems: Tools, achievements, and limitations. *Journal of Physics Condensed Matter* **28**, 1–14 (2016). 1603.04417.
- [27] Boutin, S., Andersen, C. K., Venkatraman, J., Ferris, A. J. & Blais, A. Resonator reset in circuit qed by optimal control for large open quantum systems. *Physical Review A* **96**, 042315 (2017).
- [28] Goerz, M. H. & Jacobs, K. Efficient optimization of state preparation in quantum networks using quantum trajectories. *Quantum Science and Technology* **3**, 045005 (2018).
- [29] Gautier, R., Genois, É. & Blais, A. Optimal control in large open quantum systems: The case of transmon readout and reset (2024). 2403.14765.
- [30] Murray, D. & Yakowitz, S. Differential dynamic programming and newton’s method for discrete optimal control problems. *Journal of Optimization Theory and Applications* **43**, 395–414 (1984).
- [31] Davies, E. B. Quantum stochastic processes. *Communications in Mathematical Physics* **15**, 277–304 (1969).
- [32] Carmichael, H. *An Open Systems Approach to Quantum Optics: Lectures Presented at the Université Libre de Bruxelles October 28 to November 4, 1991*, vol. 18 of *Lecture Notes in Physics Monographs* (Springer, Berlin, Heidelberg, 1993). URL <http://link.springer.com/10.1007/978-3-540-47620-7>.
- [33] Percival, I. *Quantum state diffusion* (Cambridge University Press, 1998).
- [34] Daley, A. J. Quantum trajectories and open many-body quantum systems. *Advances in Physics* **63**, 77–149 (2014). 1405.6694.
- [35] Wiseman, H. M. & Diósi, L. Complete parameterization, and invariance, of diffusive quantum trajectories for Markovian open systems. *Chemical Physics* **268**, 91–104 (2001). quant-ph/0012016.
- [36] Dalibard, J., Castin, Y. & Mølmer, K. Wave-function approach to dissipative processes in quantum optics. *Physical review letters* **68**, 580 (1992).
- [37] Dum, R., Zoller, P. & Ritsch, H. Monte carlo simulation of the atomic master equation for spontaneous emission. *Physical Review A* **45**, 4879 (1992).
- [38] Gisin, N. & Percival, I. C. The quantum-state diffusion model applied to open systems. *Journal of Physics A: Mathematical and General* **25**, 5677 (1992).
- [39] Barchielli, A. & Gregoratti, M. *Quantum Trajectories and Measurements in Continuous Time: The Diffusive Case*, vol. 782 of *Lecture Notes in Physics* (Springer Berlin Heidelberg, Berlin, Heidelberg, 2009).
- [40] Hudson, R. L. & Parthasarathy, K. R. Quantum Itô’s formula and stochastic evolutions. *Communications in mathematical physics* **93**, 301–323 (1984).
- [41] Parthasarathy, K. R. *An introduction to quantum stochastic calculus*, vol. 85 (Birkhäuser, 2012).
- [42] Belavkin, V., Hirota, O. & Hudson, R. L. *Quantum communications and measurement* (Springer Science & Business Media, 2013).
- [43] Barchielli, A. & Belavkin, V. P. Measurements continuous in time and a posteriori states in quantum mechanics. *Journal of Physics A: Mathematical and General* **24**, 1495 (1991).
- [44] Diósi, L. & Strunz, W. T. The non-markovian stochastic schrödinger equation for open systems. *Physics Letters A* **235**, 569–573 (1997).
- [45] Gambetta, J. & Wiseman, H. M. Non-markovian stochastic schrödinger equations: Generalization to real-valued noise using quantum-measurement theory. *Physical Review A* **66**, 012108 (2002).
- [46] Murch, K. W., Weber, S. J., Macklin, C. & Siddiqi, I. Observing single quantum trajectories of a superconducting quantum bit. *Nature* **502**, 211–214 (2013). URL <https://www.nature.com/articles/nature12539>. Publisher: Nature Publishing Group.

- [47] Campagne-Ibarcq, P. *et al.* Observing Quantum State Diffusion by Heterodyne Detection of Fluorescence. *Physical Review X* **6**, 011002 (2016). URL <https://link.aps.org/doi/10.1103/PhysRevX.6.011002>. Publisher: American Physical Society.
- [48] Ficheux, Q., Jezouin, S., Leghtas, Z. & Huard, B. Dynamics of a qubit while simultaneously monitoring its relaxation and dephasing. *Nature Communications* **9**, 1926 (2018). URL <https://www.nature.com/articles/s41467-018-04372-9>. Publisher: Nature Publishing Group.
- [49] Mineev, Z. K. *et al.* To catch and reverse a quantum jump mid-flight. *Nature* **570**, 200–204 (2019). URL <https://www.nature.com/articles/s41586-019-1287-z>. Publisher: Nature Publishing Group.
- [50] Wieczorek, W. *et al.* Optimal State Estimation for Cavity Optomechanical Systems. *Physical Review Letters* **114**, 223601 (2015). URL <https://link.aps.org/doi/10.1103/PhysRevLett.114.223601>. Publisher: American Physical Society.
- [51] Rossi, M., Mason, D., Chen, J. & Schliesser, A. Observing and Verifying the Quantum Trajectory of a Mechanical Resonator. *Physical Review Letters* **123**, 163601 (2019). URL <https://link.aps.org/doi/10.1103/PhysRevLett.123.163601>.
- [52] Thomas, R. A. *et al.* Entanglement between distant macroscopic mechanical and spin systems. *Nature Physics* **17**, 228–233 (2021). URL <https://www.nature.com/articles/s41567-020-1031-5>. Publisher: Nature Publishing Group.
- [53] Wiseman, H. M. & Milburn, G. J. Quantum theory of optical feedback via homodyne detection. *Physical Review Letters* **70**, 548 (1993).
- [54] Belavkin, V. Theory of the control of observable quantum systems. *Automatica and Remote Control* **44**, 178–188 (1983).
- [55] Wiseman, H. M. & Milburn, G. J. *Quantum measurement and control* (Cambridge university press, 2009).
- [56] Pham, H. *Continuous-time stochastic control and optimization with financial applications*, vol. 61 (Springer Science & Business Media, 2009).
- [57] Yong, J. & Zhou, X. *Stochastic controls. Hamiltonian Systems and HJB Equations* (Springer, 1999).
- [58] Doherty, A. C. & Jacobs, K. Feedback control of quantum systems using continuous state estimation. *Physical Review A* **60**, 2700–2711 (1999). URL <https://link.aps.org/doi/10.1103/PhysRevA.60.2700>.
- [59] Doherty, A. C., Habib, S., Jacobs, K., Mabuchi, H. & Tan, S. M. Quantum feedback control and classical control theory. *Physical Review A - Atomic, Molecular, and Optical Physics* **62**, 13 (2000). [quant-ph/9912107](https://arxiv.org/abs/quant-ph/9912107).
- [60] Bensoussan, A. *Stochastic control of partially observable systems* (Cambridge University Press, 1992).
- [61] Kraus, K., Böhm, A., Dollard, J. D. & Wootters, W. *States, Effects, and Operations Fundamental Notions of Quantum Theory: Lectures in Mathematical Physics at the University of Texas at Austin* (Springer, 1983).
- [62] Aharonov, Y., Albert, D. Z. & Vaidman, L. How the result of a measurement of a component of the spin of a spin- $1/2$ particle can turn out to be 100. *Physical Review Letters* **60**, 1351–1354 (1988). URL <https://link.aps.org/doi/10.1103/PhysRevLett.60.1351>.
- [63] Hatridge, M. *et al.* Quantum back-action of an individual variable-strength measurement. *Science* **339**, 178–181 (2013).
- [64] Aleksandrov, I. V. The Statistical Dynamics of a System Consisting of a Classical and a Quantum Subsystem. *Zeitschrift für Naturforschung A* **36**, 902–908 (1981). URL <https://www.degruyter.com/document/doi/10.1515/zna-1981-0819/html>. Publisher: De Gruyter.
- [65] Blanchard, P. & Jadczyk, A. Events and piecewise deterministic dynamics in event-enhanced quantum theory. *Physics Letters A* **203**, 260–266 (1995). URL <https://www.sciencedirect.com/science/article/pii/0375960195004323>.

- [66] Layton, I., Oppenheim, J. & Weller-Davies, Z. A healthier semi-classical dynamics (2023). URL <http://arxiv.org/abs/2208.11722>. ArXiv:2208.11722 [gr-qc, physics:hep-th, physics:quant-ph].
- [67] Diósi, L. Hybrid completely positive Markovian quantum-classical dynamics. *Physical Review A* **107**, 062206 (2023). URL <https://link.aps.org/doi/10.1103/PhysRevA.107.062206>. Publisher: American Physical Society.
- [68] Gisin, N. Quantum Measurements and Stochastic Processes. *Physical Review Letters* **52**, 1657–1660 (1984). URL <https://link.aps.org/doi/10.1103/PhysRevLett.52.1657>. Publisher: American Physical Society.
- [69] Diósi, L. Continuous quantum measurement and It^o formalism. *Physics Letters A* **129**, 419–423 (1988). URL <http://arxiv.org/abs/1812.11591>. ArXiv:1812.11591 [quant-ph].
- [70] Kappen, H. Linear theory for control of non-linear stochastic systems. *Physical Review letters* **95**, 200201 (2005).
- [71] Kappen, H. & Ruiz, H. Adaptive importance sampling for control and inference. *Journal of Statistical Physics* 10.1007/s10955–016–1446–7 (2016).
- [72] Thijssen, S. & Kappen, H. J. Path integral control and state-dependent feedback. *Phys. Rev. E* **91**, 032104 (2015). URL <http://link.aps.org/doi/10.1103/PhysRevE.91.032104>. <http://arxiv.org/abs/1406.4026>.
- [73] Williams, G., Drews, P., Goldfain, B., Rehg, J. M. & Theodorou, E. A. Aggressive driving with model predictive path integral control. In *Robotics and Automation (ICRA), 2016 IEEE International Conference on*, 1433–1440 (IEEE, 2016).
- [74] Kazim, M., Hong, J., Kim, M.-G. & Kim, K.-K. K. Recent advances in path integral control for trajectory optimization: An overview in theoretical and algorithmic perspectives. *Annual Reviews in Control* **57**, 100931 (2024).
- [75] Breuer, H.-P. & Petruccione, F. *The theory of open quantum systems* (Oxford University Press, USA, 2002).
- [76] Donvil, B. & Muratore-Ginanneschi, P. Unraveling-paired dynamical maps recover the input of quantum channels. *New Journal of Physics* **25**, 053031 (2023).
- [77] Barchielli, A. & Gregoratti, M. *Quantum trajectories and measurements in continuous time: the diffusive case*, vol. 782 (Springer, 2009).
- [78] Semina, I., Semin, V., Petruccione, F. & Barchielli, A. Stochastic schrödinger equations for markovian and non-markovian cases. *Open Systems & Information Dynamics* **21**, 1440008 (2014).
- [79] Van der Maaten, L. & Hinton, G. Visualizing data using t-sne. *Journal of machine learning research* **9** (2008).
- [80] Vandersypen, L. M. & Chuang, I. L. Nmr techniques for quantum control and computation. *Reviews of modern physics* **76**, 1037–1069 (2004).
- [81] Schirmer, S. G., Fu, H. & Solomon, A. I. Complete controllability of quantum systems. *Physical Review A* **63**, 063410 (2001).
- [82] Jones, J. A., Hansen, R. & Mosca, M. Quantum logic gates and nuclear magnetic resonance pulse sequences. *Journal of Magnetic Resonance* **135**, 353–360 (1998).
- [83] Meyer, D. A. & Wallach, N. R. Global entanglement in multiparticle systems. *Journal of Mathematical Physics* **43**, 4273–4278 (2002).
- [84] Chen, Y. *et al.* Accelerating quantum optimal control through iterative gradient-ascent pulse engineering. *Physical Review A* **108**, 052603 (2023).
- [85] Abdelhafez, M. R. *Quantum Optimal Control Using Automatic Differentiation*. Ph.D. thesis, The University of Chicago (2019).

- [86] Magann, A. B. *et al.* From pulses to circuits and back again: A quantum optimal control perspective on variational quantum algorithms. *PRX Quantum* **2**, 010101 (2021).
- [87] Choquette, A. *et al.* Quantum-optimal-control-inspired ansatz for variational quantum algorithms. *Physical Review Research* **3**, 023092 (2021).
- [88] Meitei, O. R. *et al.* Gate-free state preparation for fast variational quantum eigensolver simulations. *npj Quantum Information* **7**, 155 (2021).
- [89] De Keijzer, R., Tse, O. & Kokkelmans, S. Pulse based variational quantum optimal control for hybrid quantum computing. *Quantum* **7**, 908 (2023).
- [90] Kappen, H. J. & Ruiz, H. C. Adaptive Importance Sampling for Control and Inference. *Journal of Statistical Physics* **162**, 1244–1266 (2016). 1505.01874.
- [91] Bartholomew-Biggs, M., Brown, S., Christianson, B. & Dixon, L. Automatic differentiation of algorithms. *Journal of Computational and Applied Mathematics* **124**, 171–190 (2000).
- [92] Kappen, H. J. Path integrals and symmetry breaking for optimal control theory. *Journal of Statistical Mechanics: Theory and Experiment* 205–229 (2005). physics/0505066.
- [93] Thijssen, S. & Kappen, H. J. Path integral control and state-dependent feedback. *Physical Review E - Statistical, Nonlinear, and Soft Matter Physics* **91** (2015). 1406.4026.
- [94] Guilmin, P., Gautier, R., Bocquet, A. & Genois, É. Dynamiqs: an open-source python library for gpu-accelerated and differentiable simulation of quantum systems (2024). URL <https://github.com/dynamiqs/dynamiqs>.
- [95] Bukov, M. *et al.* Reinforcement Learning in Different Phases of Quantum Control. *Physical Review X* **8**, 031086 (2018). URL <http://arxiv.org/abs/1705.00565>. ArXiv:1705.00565 [cond-mat, physics:quant-ph].